UHASSELT
KNOWLEDGE IN ACTION

Maastricht University

Faculty of Medicine and Life Sciences
School for Life Sciences
Master of Biomedical Sciences

Master's thesis

Bio-functionalization of double network hydrogel scaffolds for cartilage tissue engineering

Valentino Atella

Thesis presented in fulfillment of the requirements for the degree of Master of Biomedical Sciences, specialization Bioelectronics and Nanotechnology

SUPERVISOR :
Prof. dr. Louis PITET

CO-SUPERVISOR :
Prof. dr. Geert-Jan GRAULUS

MENTOR :
De heer Sander DRIESEN

2022
2023

Transnational University Limburg is a unique collaboration of two universities in two countries: the University of Hasselt and Maastricht University.

UHASSELT
KNOWLEDGE IN ACTION

www.uhasselt.be
Universiteit Hasselt
Campus Hasselt:
Martelarenlaan 42 | 3500 Hasselt
Campus Diepenbeek:
Agoralaan Gebouw D | 3590 Diepenbeek

UHASSELT
KNOWLEDGE IN ACTION

Maastricht University

Faculty of Medicine and Life Sciences
School for Life Sciences
Master of Biomedical Sciences

Master's thesis

Bio-functionalization of double network hydrogel scaffolds for cartilage tissue engineering

Valentino Atella

Thesis presented in fulfillment of the requirements for the degree of Master of Biomedical Sciences, specialization Bioelectronics and Nanotechnology

SUPERVISOR :
Prof. dr. Louis PITET

MENTOR :
De heer Sander DRIESEN

CO-SUPERVISOR :
Prof. dr. Geert-Jan GRAULUS

Bio-functionalization of double network hydrogel scaffolds for cartilage tissue engineering*

Atella V[1], Driesen S[2,3], Graulus G-J[3], and Pitet L[2]

[1]Master student Biomedical Sciences – Bioelectronics & Nanotechnology, Hasselt University, Agoralaan, building D, 3590 Diepenbeek, Belgium

[2]Advanced Functional Polymers (AFP) Group, Department of Chemistry, Institute for Materials Research (IMO-imomec), Hasselt University, Agoralaan, building D, 3590 Diepenbeek, Belgium

[3]Biomolecule Design Group (BDG), Department of Chemistry, Institute for Materials Research (IMO-imomec), Hasselt University, Agoralaan, building D, 3590 Diepenbeek, Belgium

**Running title: Bio-functionalization of double network hydrogels*

To whom correspondence should be addressed: L. Pitet; Email: louis.pitet@uhasselt.be

Keywords: Double-network hydrogel, Bio-functionalization, Alginate sulfate, Cartilage, Tissue engineering, Mechanical testing

ABSTRACT

Osteoarthritis is a global health concern that affects 500 million people and arises from the breakdown of joint articular cartilage. Tissue engineering could provide an advanced treatment by stimulating the limited natural regeneration that stems from the lack of vascularization and finite cellular tissue. An important factor in designing a scaffold is its ability to effectively dampen the mechanical energy around the damaged area. To achieve this, the hydrogel must be adequately tough to mimic the high stiffness of the articular cartilage. Advancements in scaffold design have led to double-network (DN) hydrogels, which display enhanced toughness. However, many of these scaffolds lack the functionality to stimulate tissue regeneration. This is why this research sets out to create a bioactive poly(acrylamide-co-acrylic acid)/alginate sulfate DN hydrogel. These hydrogels are synthesized via the radical-mediated covalent crosslinking of acrylamide and acrylic acid and the ionic crosslinking of alginate sulfate. Alginate sulfation is achieved via the reaction with chlorosulfonic acid. FTIR, ^{13}C-NMR, and element analysis confirmed the successful sulfation, achieving a degree of sulfation of 0.85. Mechanical testing showed that DN hydrogels, with a water content of 75 % and an alginate content of 2 wt%, results in a compressive stiffness of 230 kPa, which is similar to the compressive stiffness of native cartilage. Cyclical mechanical testing also showed the resilience and extreme toughness of the hydrogel under continuous deformation. These results create the fundamental knowledge required to further enhance the mechanical and bioactive capabilities of this hydrogel scaffold system.

■ INTRODUCTION

Hydrogels are three-dimensional crosslinked polymeric hydrophilic structures, designed to swell and contain large amounts of water (1, 2). They are ideal for biomedical applications due to their unique properties: biocompatibility, biodegradability, flexibility, resemblance to living tissue, and ease of use (1, 2). One of these prominent biomedical applications is tissue engineering. A multidisciplinary field focused on the regeneration of damaged tissue by combining biology, biochemistry, material science, and clinical medicine (3). Hydrogel scaffolds play a crucial role in tissue regeneration due to their resemblance to the extracellular matrix (ECM) (3, 4). Their specific physical, chemical, and biological characteristics can be fine-tuned to resemble the ECM of the targeted tissue to induce regeneration (3).

One of the frequently targeted tissues is articular cartilage due to its limited ability for regeneration that stems from the lack of vascularization and finite cellular tissue (3, 5-7). The current restrictions of cartilage surgery such as complicated surgical procedures, quality of the regenerated cartilage, and post-surgery infections, provide an opportunity for tissue engineering to advance cartilage tissue treatment (5, 6). The main role of cartilage is to create a low-friction area inside joints to allow for unhindered motion. The composition and structure of cartilage tissue are depth-dependent, but generally, cartilage consists of water (70-85%), various types of collagens (10-18%), proteoglycans (5-9%), and chondrocytes (3-6%) (5, 6). It is this composition that gives cartilage its load-bearing properties of high stiffness (≥1 MPa), high tensile resistance (15-35 MPa), and compressive strength (15-35 MPa) (5, 6). An important factor in designing a cartilage scaffold is that it can effectively dampen the mechanical energy around the damaged area. To achieve this, the hydrogel must be adequately tough to mimic the high stiffness of the cartilage (5, 6).

Many past studies have focused on identifying new complex hydrogels that mimic cartilage. However, their success varies widely due to factors such as cell viability, adhesion and proliferation, shape fidelity, controllable porosity, toxic gelation agents, and gelation time (5). The most successful of these new complex hydrogels are nanocomposite hydrogels, multi-material hydrogels, sliding ring hydrogels, and double network (DN) hydrogels. Among these, DN hydrogels have been

demonstrated to achieve extremely high mechanical strength and toughness (5, 8, 9). These superior mechanical properties emerge from the interpenetration of two polymer networks with contrasting properties. The first network is usually brittle, rigid, and highly cross-linked, which will dissipate large amounts of energy by sacrificing many of its cross-linking bonds. In contrast, the second network is often ductile, soft, and weakly cross-linked and will absorb external stress to make the hydrogel maintain its shape (8, 9). In the early stages of DN hydrogel research, chemically crosslinked networks were mainly synthesized. When these were stretched, the first rigid, strongly crosslinked network permanently broke into fragments to dissipate energy. This sacrifice of covalent bonds results in irreversible damage and a sharp permanent decrease in mechanical strength (8, 9). To solve this problem, dynamic and reversible physical bonding was adopted. These include crosslinking bonds formed via ionic interactions, van der Waals forces, hydrogen bonds, hydrophobic associations, etc. In contrast to the permanent breaking of bonds in the fully chemically DN hydrogels, the hybrid physically/chemically DN hydrogels show a continuous energy dissipation mechanism. Since non-covalent bonds are involved all hybrid gels often exhibit good reversibility and recoverability of the network (8, 9). This reversibility and recoverability combined with extremely high mechanical strength and toughness make the hybrid physically/chemically DN hydrogels one of the most used hydrogel types in cartilage tissue engineering.

Selecting the optimal materials to create a though physically/chemically crosslinked DN hydrogel is no easy task. Generally, the polymeric materials used in tissue engineering can be divided into either synthetic materials or natural materials. The most widely used synthetic polymers are polyesters, vinyl polymers, and polyethylene glycol (PEG) (10). Of these synthetic materials, a few specific polymers are attractive for cartilage tissue engineering, namely PEG, polycaprolactone (PCL), poly(vinyl alcohol) (PVA), and poly(acrylamide). Poly(acrylamide) forms stable, biocompatible, and bioinert hydrogels and is widely used as a filler for damaged cartilage tissue in certain parts of the world, especially in Asia (10, 11). Furthermore, the incorporation of co-monomers, such as acrylic acid, can also readily be done to create acrylamide copolymers with different properties (10). Hydrogels based on acrylic acid and acrylamide are superabsorbent and have been used for various biomedical and tissue engineering applications (12). Therefore, this research will focus on further developing these networks for cartilage tissue engineering. Poly(acrylamide-co-acrylic acid) (poly(AAm-co-AAc)) hydrogels are fabricated via a free radical polymerization mechanism. Generally, free radical polymerization combines ammonium persulfate (APS) and tetramethylethylenediamine (TEMED) for the free radical initiation process. These free radicals affect the double bonds present in the monomers (acrylic acid and acrylamide) and the cross-linking agent (methylene-bis-acrylamide (MBAA)) bonding them to one another via covalent bonds to form a solid gel (12).

Covalently crosslinked poly(acrylamide) networks have already been combined with ionically crosslinked networks to yield a physically/chemically crosslinked DN hydrogel. The poly(acrylamide)/alginate DN hydrogel was first reported by Suo et al. in 2012 (13). Their findings show that combining poly(acrylamide) and alginate networks is extremely promising for cartilage tissue engineering. The aforementioned reported maximum fracture energy of 8,700 J/m^2 and a stretchability beyond 20 times the initial length (13). These findings demonstrate that a physically/chemically crosslinked DN hydrogel composed of poly(acrylamide) and alginate is extremely tough and suitable to function as a cartilage scaffold. Alginates are unbranched linear copolymers composed of 1,4-linked mannuronic acid (M) and guluronic acid (G) and can be isolated from brown algae. Alginate gelation occurs when polyvalent cations, such as Ca^{2+}, interact with G blocks to form ionic crosslinking bonds. Alginate also has a few considerable advantages; it is biocompatible, has suitable porosity, easily forms gels, and is a natural material (14). Additionally, alginates have been used as synthetic extracellular matrices for cell encapsulation and proliferation (14, 15).

However, other factors besides selecting the optimal materials to match the mechanical properties of cartilage are also crucial in engineering a hydrogel scaffold for cartilage regeneration. Cell differentiation, cell adhesion, and integration into the native cartilage are all important to facilitate tissue regeneration (5, 16). To achieve these bioactive properties, cell adhesion ligands and epitopes for cell-surface interactions could be added to the scaffolds (5, 16). Adding proteins, peptides, or growth factors to a hydrogel scaffold, or functionalities that mimic these, would provide the required biochemical signaling to improve tissue regeneration. A major component of the native cartilage ECM is chondroitin sulfate (CS). CS is a sulfated glycosaminoglycan (GAG) comprised of alternating N-acetylgalactosamine and glucuronic acid, with variable sulfation along the polysaccharide (17). CS is responsible for many of the important biomechanical properties of cartilage, such as resistance and elasticity allowing cartilage to resist stresses during various conditions (17-19). Furthermore, they also play a vital role in the development, maintenance, and pathophysiology of tissues, and may serve as receptors, co-receptors, and reservoirs of proteins and growth factors through electrostatic interaction (17, 20-22). CS has been used for medical purposes for over 40 years and is sold as an over-the-counter dietary supplement in North America and as a prescription drug in Europe (18). Therefore, the introduction of sulfate moieties on the alginate network will allow the hydrogel to mimic CS. The alginate sulfate can serve as a reservoir and a slow-release system for growth factors aimed toward tissue regeneration (20, 22). Multiple strategies have been described for the sulfation of alginate. One common method is the chlorosulfonic acid-mediated sulfation of alginate in formamide,

routinely employed due to ease of reaction, low batch-to-batch variation, and good reaction controllability (23). However, the strongly acidic environment may result in partial depolymerization and reduced reproducibility. An alternative strategy to combat this limitation is the reaction between alginate and the uncommon sulfating agent $N(SO_3Na)_3$ in an aqueous solution (24). It has already been shown that the addition of these sulfate moieties results in enhanced proliferation and long-term viability of chondrocytes further enhancing the cartilage tissue engineering capabilities of alginate-containing hydrogel (20, 22).

As of yet, no high-impact studies have been conducted on the design and synthesis of bioactive double-network hydrogels for cartilage tissue engineering. There is a clear need for new advanced cartilage tissue treatment as the current treatment of osteoarthritis is very restricted due to the complicated surgical procedures, low quality of the regenerated cartilage, and high prevalence of post-surgery infections. This is why this research will design a bioactive poly(acrylamide-co-acrylic acid)/alginate sulfate double network hydrogel to combat this niche but important problem. Two alginate sulfation strategies, namely the reaction with $N(SO_3Na)_3$ and the reaction with chlorosulfonic acid, will be explored to yield a bioactive alginate sulfate network. This network will be combined with poly(acrylamide-co-acrylic acid) to yield a tough double network hydrogel, that is suitable for the regeneration of articular cartilage.

■ MATERIALS AND METHODS

Reagents

Sodium alginate, N,N'-methylene bisacrylamide (MBAA), and ammonium persulfate (APS) were purchased from Sigma-Aldrich, U.S.A. Sodium nitrite, chlorosulfonic acid, and formamide were purchased from Thermo Fisher Scientific, U.S.A. Acrylamide (AAm), tetramethylethylenediamine (TEMED), sodium bisulfite, Iron(III) chloride ($FeCl_3$), calcium chloride ($CaCl_2$), and calcium sulfate ($CaSO_4$) were purchased from Acros Organics, U.S.A. Iron sulfate ($FeSO_4$) and magnesium sulfate ($MgSO_4$) were purchased from VWR Chemicals, U.S.A. Copper sulfate ($CuSO_4$) was purchased from Janssen Chimica, Belgium. Activated charcoal and aluminum chloride ($AlCl_3$) were purchased from Merck KGaA, Germany. Acrylic acid was purchased from J&K Scientific, U.S.A. Deuterated water (D_2O) was purchased from Cambridge Isotope Laboratories, U.K. All chemicals were used as received unless stated otherwise.

Alginate functionalization

Alginate purification

Before use in functionalization reactions, the commercial sodium alginate is purified with activated charcoal. The sodium alginate was dissolved in milli-Q water (0.01 g/ml) at 4 °C for at least 24 h. Afterward, the activated charcoal was added to the solution in a 1:2 ratio compared to the alginate. The solution was left to stir for 24 h at 4°C to allow for the adsorption of any impurities. Then the activated charcoal is removed from the solution by first centrifuging 50 ml aliquots at 7000 rcf for 20 min at 10 °C. The decanted solution is then further filtrated in a Buchner funnel under vacuum through 1.2, 0.8, 0.45, and 0.2 µm Whatman membrane filters. The remaining water was then removed by lyophilization to yield purified white fibrous alginate.

Alginate sulfation

Alginate sulfate was synthesized through the reaction with chlorosulfonic acid in formamide. Alginate sulfate was dissolved in a 20 vol% solution of chlorosulfonic acid in formamide in a three-arm round-bottom flask equipped with a condenser, and magnetic stirring. The solution was then heated to 60 °C and left to react for 4 h. Afterwards the alginate sulfate was precipitated in cold acetone and filtrated before redissolving in demineralized water. The solution was then neutralized with NaOH (2 M) and dialyzed (6-8 kDa) with demineralized water (48 h), and finally, lyophilized.

Alternatively, alginate sulfate was also synthesized via the reaction with the sulfating agent $N(SO_3Na)_3$. $N(SO_3Na)_3$ was obtained through the reaction between sodium bisulfite and sodium nitrate (4.25:1 molar ratio) in a three-arm round-bottom flask equipped with a condenser, and magnetic stirring. An aqueous solution of sodium nitrite was added dropwise to the aqueous sodium bisulfite solution at 90 °C for 1.5 h while stirring. In this way, the sulfating agent was obtained. Then, the pH of sulfating agent solution was adjusted to 9 using NaOH (2 M), and purified sodium alginate (5 g) was added. The sulfating reaction was allowed to proceed for 4 h at 40 °C while stirring. The resulting solution was then neutralized using HCl (6 M), dialyzed (6-8 kDa) with demineralized water (48 h), and lyophilized.

Alginate characterization

Gel permeation chromatography

Gel permeation chromatography (GPC) was performed to assess the effects of the alginate purification process. Samples were prepared by dissolving 5 mg of the product in 5 ml of a 0.1 M $NaNO_3$ solution. Aqueous GPC measurements were made on a Shimadzu Prominence LC purchased from Shimadzu Corporation, Japan. Measurements were performed using water (0.1 M $NaNO_3$) as the mobile phase on a Tosoh. G4000PWXL column (7.8 x 300 mm) and a flow rate of 0.4 mL/min. Eluograms were converted to molar mass (MW) distributions using calibration data from poly(ethylene glycol) standards. GPC data was processed with Igor Pro 8 software from WaveMetrics.

^{13}C-NMR analysis

Carbon-nuclear magnetic resonance spectroscopy (^{13}C-NMR) was performed to assess alginate functionalization. Samples were prepared by dissolving 40-80 mg of the product in 1.2 ml deuterated water (D_2O). Tetramethylsilane (TMS) was used as an internal standard. All NMR measurements were analyzed using MNova software from Mestrelab Research.

FTIR spectroscopy

Fourier-transformed infrared (FTIR) spectroscopy was performed to assess alginate functionalization. The spectra were recorded using a Spectrum 3 FT-IR spectrometer equipped with a diamond ATR prism purchased from PerkinElmer, U.S.A. The spectra were made in the spectral region from 4000 cm^{-1} to 600 cm^{-1} at a resolution of 4 cm^{-1}. FTIR data was processed with Igor Pro 8 software from WaveMetrics.

Element analysis

The carbon, hydrogen, nitrogen and sulfur contents were measured by the elemental analysis method via a FLASH 2000 CHNS/O analyzer purchased from Thermo Fisher Scientific, U.S.A. The degree of sulfation (DS), number of sulfate groups per monomer, was calculated using the following formula (24, 25):

$$DS = \frac{198[S]}{(3200 - 102[S])}$$

where [S] was the sulfur content (%) of alginate sulfate obtained from the element analysis.

DN hydrogel synthesis

Two-step hydrogel preparation

Various poly(AAM-co-AA)/alginate double network hydrogel formulations (Table S1) were synthesized via a two-step solution-gel procedure. The process starts with forming a homogeneous solution of the network components in demineralized water at room temperature. First, the sodium alginate (1, 2, or 3 wt%) was dissolved in the desired volume of demineralized water at room temperature. Then the acrylamide (AAm) and the acrylic acid (AA) with various AAm:AA ratios (80:20 or 90:10) were added to the solution while stirring. In the first crosslinking step, the poly(AAM-co-AA) network was formed via radical copolymerization/cross-linking. To this end, the crosslinker, MBAA (0.05 mol% relative to AAm & AA), the radical initiator APS (0.80 mol% relative to AAm & AA), and the accelerator TEMED (76.37 mol% relative to APS) were added. The solution was then stirred for ~1 min before transferring to a PMMA mold. The solution was then left to gel overnight. In the second crosslinking step, the alginate network was ionically crosslinked. The gels were carefully removed from the PMMA mold and immersed into a 0.3 M aqueous solution of calcium chloride for 2 hours. The ionic crosslinking step was also performed with other compounds ($FeCl_3$, $FeSO_4$, $AlCl_3$, $CuSO_4$, $MgSO_4$) using the same procedure as described above.

One-step hydrogel preparation

Various poly(AAM-co-AA)/alginate (sulfate) double network hydrogel formulations (Table S1) were synthesized via a one-step solution-gel procedure. The process proceeds as described above by first forming a homogeneous solution of the network components. Then, in the first crosslinking step both the poly(AAM-co-AA) and alginate networks were formed. The formation of the poly(AAM-co-AA) remains unaltered while the formation of the alginate network was simultaneously induced by the addition of calcium sulfate (13.28 wt% relative to alginate). The solution was then transferred to a PMMA mold and left to gel overnight.

Swelling tests

The synthesized poly(AAM-co-AA)/alginate hydrogels were weighed in a glass vial and submerged in deionized water (5 ml) at room temperature. The gels were then allowed to swell to a constant equilibrium mass (48 h), and their swelling was documented by weighing the swelling gels every two hours. The water content was calculated using the following equation:

$$\text{Water content}\,(\%) \;=\; 1 - \frac{(\mathrm{m_i} \cdot 0.25)}{\mathrm{m_t}}$$

with m_t the mass at time t and m_i the initial mass.

After swelling to a constant equilibrium mass the gels were dried overnight to a constant dried mass at 50 °C under vacuum. The mass swelling ratio (q) was then defined using the following equation:

$$\mathrm{q} = \frac{\mathrm{m_t} - \mathrm{m_0}}{\mathrm{m_0}}$$

with m_t the mass at time t and m_0 the dried mass.

Mechanical tests

The mechanical properties of hydrogels were tested by uniaxial tensile tests and uniaxial unconfined compression tests. Both tests were done with an autograph AGS-X and its accompanying software TrapeziumX purchased from Shimadzu Corporation, Japan. All hydrogels for compression testing were made in cylindrical PMMA molds (diameter: 8 mm; height: 3 mm), while all hydrogels for tensile testing were made in dogbone PMMA molds (gauge length: 10 mm; width: 3.5 mm; height: 2.15 mm). Compression tests were done with a load cell of 5 kN and a strain speed of 1 mm/min up to 90% strain. Cyclical compression tests were done with a load cell of 5 kN for 20 cycles with a downward strain speed of 5 mm/min and an upward strain speed of 10 mm/min up to 90% strain. Tensile testing was done with a load cell of 500 N and a strain speed of 50 mm/min until gel rupture.

Compression and tensile testing data were processed with Igor Pro 8 software from WaveMetrics. The elastic and compressive moduli were calculated by determining the slope of the linear region (10-20 % strain) of the stress-strain curve.

Statistical analysis

All data are reported as mean ± standard deviation (SD). For each experiment, three samples were analyzed. Statistical differences (p-value ≤ 0.05) between multiple groups were determined by using the one-way ANOVA test with post hoc Tukey's test. While statistical differences (p-value ≤ 0.05) between two groups were determined using the two-sided Student's t-test. All statistical analyses were done with GraphPad Prism 9 software from Dotmatics.

■ RESULTS AND DISCUSSION

Poly(AAM-co-AA)/alginate DN hydrogel

Swelling properties

Six different poly(AAM-co-AA)/alginate DN hydrogels formulations (Table S1) were synthesized according to the two-step solution-gel method. The swelling properties of these formulations were evaluated by submerging them in deionized water until an equilibrium mass was achieved. The increase in water content from the initial 75 wt% (synthesis condition) to equilibrium water content is shown in Figure 1A. Equilibrium mass is achieved for all formulations after 24 h of swelling as a plateau is reached that persist for another 24 h giving the end of measurements at 48 h. Both the A and B variants of the six formulations show an increase in the equilibrium water content as the amount of alginate decreases. This trend is also indicated by the mass swelling ratio at equilibrium (Figure 1B), the ratios decrease as the amount of alginate increases. However, the statistical analysis indicates that only 1B is significantly different from 1A (p-value = 0.031), 2A (p-value = 0.009), and 3B (p-value = 0.014). The observed differences and trends are thus not very strongly pronounced. The trend is explained by the rigid ionic alginate network increasing the crosslinking density of the hydrogel which results in a decrease in the swelling capabilities. This is to be expected as it is now that several physicochemical parameters such as solvent nature, network density, the interaction of polymer-solvent, and particularly the extent of porosity mainly impact the swelling behavior (26-28). Hydrogel porosity is conventionally categorized into four different groups: non-porous, macroporous, microporous, and super porous hydrogels (26, 27). This grouping is based on the packing density of the polymer chains which limits the diffusion of solvent through the matrix. This packing density is mostly influenced by the crosslinking of the hydrogel (26, 27). Thus, increasing the rigid, densely crosslinked alginate decreases the porosity and increases the packing density of the polymer chains, as a result, the swelling ratios decrease.

However, the poly(AAM-co-AA) network composition also impacts the swelling behavior as the mass swelling ratios (Figure 1B) show that the B variants swell to a slightly larger degree than the A variants, although, only significantly for 1A & B. This is also visible in the upward shift of the B variant compared to the A variants when looking at the change in water content (Figure 1A). The results indicate that the swelling ratio increases when [AAm] increases and [AA] decreases. This difference in swelling behavior is related to osmosis, the driving force in swelling for hydrogels possessing ionic groups (29, 30). The poly(AAM-co-AA) network possesses carboxyl and amine groups, which become ionized as the pH of the solvent is above the pKa of the carboxyl group and below the pKb value of the amine groups. At pH 7 (deionized water) both types of groups are in ionized form and contribute to water absorption (29, 30). Most studies show that at pH 7 the ionization degree and

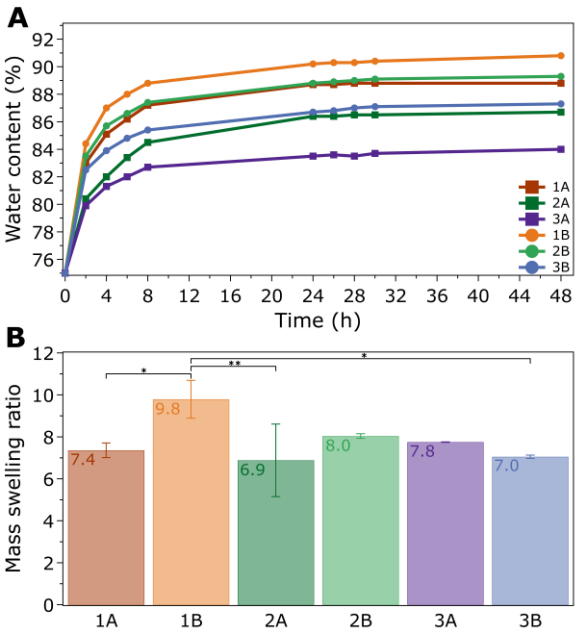

Figure 1 Swelling properties of the six DN hydrogels. (A) Water content change. The water content increases as the amount of alginate decreases for both variants, indicating decreasing swelling capabilities as the crosslinking density rises. The B variants of each formulation are shifted upward indicating stronger swelling capabilities as the amount of acrylamide increases and acrylic acid decreases. **(B)** Mass swelling ratio at 48 h. The ratios indicate that the hydrogels are capable of absorbing 7-10 times their dry weight in water. The ratios also seem slightly higher for the B variants, indicating increased swelling capabilities as the amount of acrylamide increases and acrylic acid decreases. However, only formulation 1B displayed a significantly higher mass swelling ratio as indicated.
** = P ≤ 0.05, ** = P ≤ 0.01*

contribution of the carboxyl groups are greater. Thus, a higher degree of acrylic acid should result in a higher swelling ratio, which is not supported by the results reported here (29-31). However, the ionized carboxyl groups of the acrylic acid monomers can interact with the calcium ions and form crosslinks thereby diminishing the hydrogel porosity (32-34). Therefore, as the ratio AAm:AA increases the number of carboxyl groups is decreased and the crosslinking density decreases resulting in a higher degree of swelling. These interactions between the ionized groups, calcium ions, and water molecules are thus the basis for the observed difference between A and B hydrogel variants. Based on these results it was determined that formulations 2A and 3A are the most suitable for cartilage tissue engineering as their equilibrium water content is ~87 and ~84% water, respectively. This matches the composition of cartilage tissue (70-85% water) the strongest (5).

Mechanical properties

Six different poly(AAM-co-AA)/alginate DN hydrogel formulations (Table S1) were synthesized according to a two-step and one-step solution-gel method. The mechanical properties of these formulations were evaluated in both tensile and compression tests. The tensile and compressive

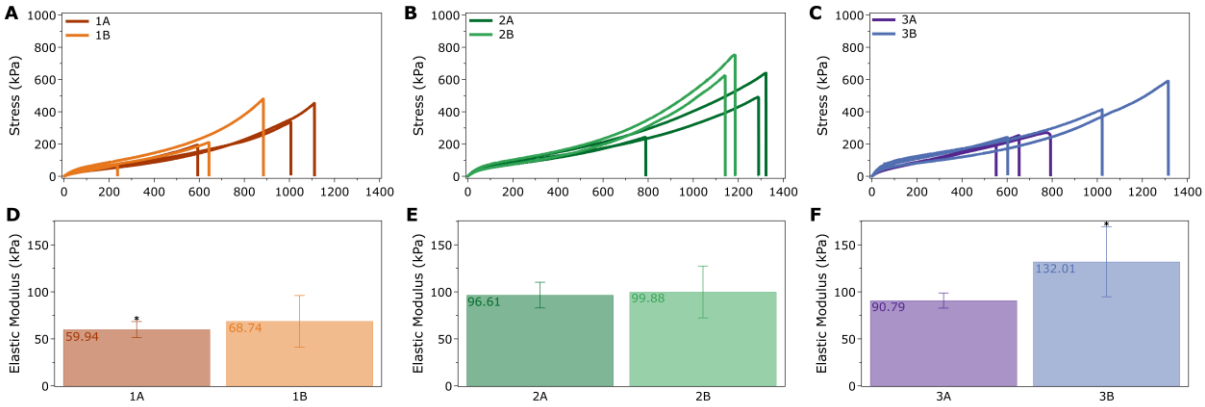

Figure 2 Tensile properties of the six DN hydrogels synthesized via the one-step method. All hydrogels display nonlinear viscoelastic behavior. **(A-C)** Tensile stress-strain curves of the A and B variants of formulations 1, 2 and 3, respectively. A general increase in the slope of the elastic region is visible as the amount of alginate increases, indicating higher degrees of toughness. Ductility is similar for formulations 1 and 2, while formulation 3 is noticeably less ductile and more rigid. **(D-F)** Elastic modulus of the A and B variants of formulations 1, 2, and 3 respectively. The moduli of the A & B variants are similar, indicating that a change in acrylic acid content does not greatly alter the toughness. A general increase in the modulus is visible as the amount of alginate increases, indicating higher degrees of toughness. However, only the difference between the modulus of 1A and 3B is significant. ** = P ≤ 0.05*

stress–strain curves show the nonlinear viscoelastic behavior of the tough hydrogels (Figure 2, Figure 3, Figure S2, and Figure S3). Following the application of strain, elastic deformation occurs up to ~50-75% strain. As the strain further increases stress relaxation occurs due to disruption of ionic and transient physical cross-links, enabling rearrangement of the network. This is predominantly facilitated by water migration and exudation (35, 36). The Young's modulus of each hydrogel was determined within the elastic deformation region, specifically 10-20% strain.

The tensile tests were performed at a strain speed of 50 mm/min until gel rupture for all six DN hydrogels, synthesized via the two- and one-step solution-gel method. The stress–strain curves and elastic modulus of all hydrogels synthesized via the two-step method are shown in Figure S2. Formulations 1A & B reach similar average elastic moduli at 54.7 ± 8.8 and 36.6 ± 20 kPa, respectively (Figure S2D). Furthermore, these formulations are also ductile, the most stretchable gels can reach up to ~825% strain (Figure S2A). The properties of formulation 2A are similar by reaching an average elastic modulus of 50.7 ± 0.30 kPa and being elongated up to ± 650-725% strain (Figure S2B & E). Formulation 2B on the other hand displays a higher degree of toughness while remaining ductile. The average elastic modulus of 2B is 99.6 ± 1.3 kPa and the most elastic gel can reach up to ~1000 % strain (Figure S2B & E). Formulations 3A and 3B are considerably stiffer compared to the other formulations. 3A and 3B reach elastic moduli of 113 ± 16 and 140 ± 35 kPa, respectively (Figure S2F). This increased modulus also resulted in less stretchability as the most ductile gel can reach ~650% strain (Figure S2C). The statistical analysis of these values (Table S2) indicates only a significantly higher modulus for formulations 3A and 3B. Both, 3A and 3B, are significantly higher than the moduli of formulations 1A (p-value = 0.019 and 0.002), 1B (p-value = 0.004 and 0.0006), and 2A (p-value = 0.026 and 0.004). The mechanical properties do not change drastically when the hydrogels are synthesized via the one-step method. All six formulations have similar elastic moduli compared to the two-step method (Figure 2D-F). Formulations 1A & B have an average elastic modulus of 59.9 ± 8.5 and 68.7 ± 27 kPa, respectively (Figure 2D). This is slightly higher than the properties achieved via the two-step method. Formulations 2A & B reach higher average elastic moduli at 96.6 ± 14 kPa and 99.9 ± 8.1 kPa, respectively (Figure 2E). Only formulation 2A showed a substantially increased toughness compared to its two-step method counterpart. The general increasing trend in toughness continues with formulations 3A & B, which reached average elastic moduli of 90.8 ± 8.1 and 132 ± 37 kPa, respectively (Figure 2F). This is comparable to the moduli reached via the two-step method. Despite the similar moduli when compared to the two-step method, the ductility of all six formulations does increase. The most ductile gels of formulations 1A & B reach a maximum strain of ~1110 and ~884% strain (Figure 2A), respectively, which is a noticeable increase. Formulations 2A & B are even more ductile and reach a maximum strain of ~1320 and ~1180% strain (Figure 2B). This is once again a noticeable increase when compared to the two-step method. The ductility of formulations 3A & 3B increased considerably to ~790 and ~1310% strain (Figure 2C). The statistical analysis of these values (Table S3). only indicates a significant increase in the modulus of 3B compared to 1A (p-value = 0.023).

These results clearly show that the one-step method results in more ductile DN hydrogels while maintaining the toughness. Furthermore, the properties are also in line with, or superior to, results reported in the literature for poly(acrylamide)/alginate DN hydrogel systems (13, 37-40). The elastic modulus reported in the literature varies from lower ranges (50-70 kPa) to higher ranges (150-500 kPa) (13, 37-40). The results reported here are values that fit within the top of the lower ranges reported in the literature. Therefore, it can be concluded that the elastic properties displayed by the

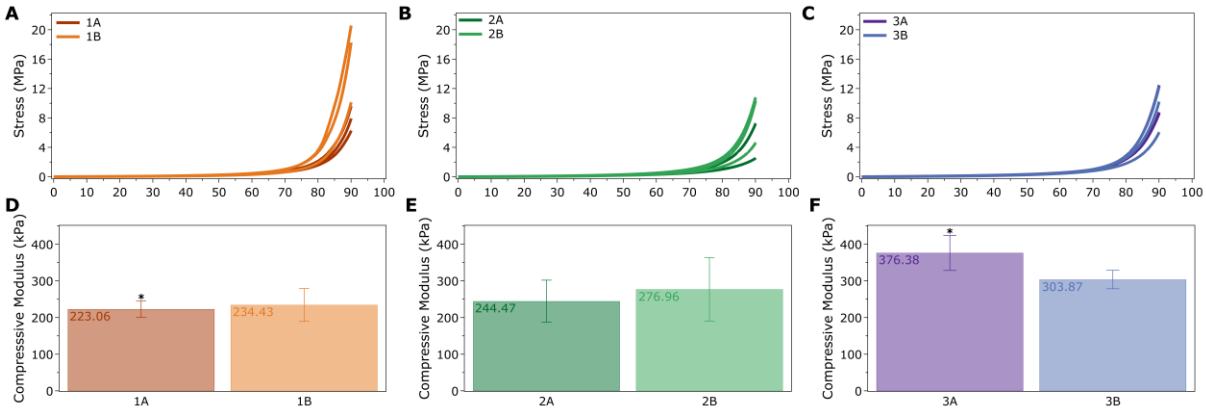

Figure 3 Compressive properties of the six DN hydrogels synthesized via the one-step method. All hydrogels display nonlinear viscoelastic behavior. **(A-C)** Compression stress-strain curves of the A and B variants of formulations 1, 2, and 3, respectively. A general increase in the slope and maximum stress is visible as the amount of alginate increases, indicating higher degrees of toughness. **(D-F)** Compressive modulus of the A and B variants of formulations 1, 2, and 3, respectively. The moduli of the A & B variants are similar, indicating that a change in acrylic acid content does not greatly alter the toughness. A general increase in the modulus is visible as the amount of alginate increases, indicating higher degrees of toughness. However, only the difference between the modulus of 1A and 3A is significant.
** = P ≤ 0.05*

various formulations are exemplary of the properties to be expected from physically/chemically crosslinked DN hydrogel. However, the tensile toughness reached by the six formulations is far below the tensile toughness of cartilage (5-25 MPa) (5, 7). Further improvement of the stiffness would thus be favorable for cartilage tissue engineering. This could be achieved through various strategies, such as: increasing the alginate G-block content, further increasing the alginate wt%, increasing the amount of MBAA, use of other multivalent ions, etc. However, the main mode of deformation and stress occurring in cartilage tissue is compressive (5, 6). Therefore, the tensile toughness of the hydrogels is of lesser importance when considering them for tissue engineering. Despite this, the extensibility of all the formulations is superior to that of cartilage (up to 1.4 times) (5). In this regard, DN hydrogels are more than suitable for tissue engineering.

The compressive properties of the six formulations were also evaluated in compression tests at a strain speed of 1 mm/min until 90% strain is reached. All formulations synthesized via the two-step solution-gel method reached 90% strain without major macroscopic damage occurring. The stress–strain curves and compressive modulus of all six DN hydrogel formulations are shown in Figure S3. Formulations 1A & B reach similar average maximum stress of 2.15 ± 0.78 and 2.18 ± 0.55 MPa, respectively (Figure S3A). Unsurprisingly, the average compressive moduli of both formulations are also similar at 118 ± 43 and 123 ± 5 kPa, respectively (Figure S3D). Formulations 2A & B reach slightly higher average maximum stress at 2.15 ± 0.55 and 3.24 ± 0.68 MPa, respectively (Figure S3B). Despite the similar maximum stress to 1A & B, the average compressive moduli of both formulations are considerably higher at 150 ± 72 and 185 ± 93 kPa (Figure S3E). The rising trend continues with formulations 3A & B reaching higher average maximum stress, 4.36 ± 0.97 and 2.36 ± 0.32 MPa (Figure S3C). Despite this increase, the average compressive modulus of both formulations 3A & B are similar to 2A & B at 149 ± 27 and 163 ± 19 kPa, respectively (Figure S3F). These values (Table S4) do, however, only describe a rising trend in the modulus matched to the increase in the wt% of alginate as the statistical analysis showed no significant differences. The same trend does hold for the formulations synthesized via the one-step solution-gel method, despite the lack of significance for the two-step method. All six formulations also reached 90 % strain without major macroscopic damage occurring. However, a major difference is that the one-step method results in a globally increased toughness. All formulations have a substantially increased modulus when compared to the two-step method (Figure 3D-F). The average compressive modulus of formulations 1A & B is 223 ± 23 and 234 ± 45 kPa, respectively (Figure 3D). Formulations 2A & B, once again, reach higher average compressive moduli at 244 ± 58 and 277 ± 87 kPa, respectively (Figure 3E). The increasing trend continues with 3A & B reaching average compressive moduli of 376 ± 48 and 304 ± 25 kPa (Figure 3F). All formulations also reach a substantially increased max stress when compared to the two-step method (Figure 3A-C). The average max stress of formulations 1A & B are 7.90 ± 2.4 and 16.3 ± 5.5 MPa, respectively (Figure 3A). Formulations 2A & B reach lower average maximum stress at 4.77 ± 2.4 and 8.55 ± 3.4 MPa (Figure 3B). However, this is still substantially higher compared to the two-step method. The average max stress of formulations 3A & B were 9.93 ± 2.2 and 9.49 ± 3.2 MPa (Figure 3C). The statistical analysis of these results (Table S5) only showed a significant difference in the moduli of 3A and 1A (p-value = 0.033)

A noticeable similarity between the two- and one-step methods is that differences in maximum stress between formulations are not logically matched by differences in compressive modulus. This could be explained by the occurrence of plastic deformation from ~50-75% strain onwards. The departure from the linear relation between stress and strain in the elastic region explains this discrepancy between the maximum stress

reached and the compressive modulus. However, the results clearly show that the one-step method results in tougher DN hydrogels. This can be attributed to the lower water content (75 wt%), as via this method, there is no additional uptake of water, unlike the two-step method. Secondly, by using the one-step method the cross-linking of the alginate network will be more effective, as the distribution of cations is more efficient when compared to the diffusion-based two-step method. Furthermore, the properties are also in line with the results reported in the literature for various poly(acrylamide)/alginate DN hydrogel systems (41-44). The max stress reported in the literature varies over a wide range from relatively low values (0.1-0.2 MPa) to moderate values (1.5-2.5 MPa) and even high values (11.5-12.5 MPa) (41-44). The results reported here fit within these ranges but are not on par with the highest reported values. Nevertheless, all six formulations, when synthesized via the one-step method, reach a compressive toughness that lies within or is close to the compressive modulus of native cartilage (0.23-0.85 MPa) (5, 7). These properties, although already formidable, could still be further enhanced through various strategies, such as variation of the ion concentration, use of other multivalent ions, increase of the alginate G-block content, nanocomposite formulations using nanoparticles, etc. Important to note is that the results are achieved via unconfined compression, which allows the hydrogels to expand laterally during the deformation. One could expect a stronger build-up of tension and resistance of the hydrogels in confined compression which would result in a measured modulus that is considerably higher (7, 45). Confined compression could therefore elucidate the compressive properties more analogously to *in vivo* deformations (7, 45). Of all six formulations, formulations 2 and 3 (both variants) display the most promising mechanical properties for cartilage tissue engineering.

When the results of both the tensile and compression tests are analyzed together, formulation 2 (both variants) displays the most promising mechanical properties. It combines ductility, high elastic toughness, and high compressive toughness. This combination of properties shows that formulation 2 displays a more rounded and versatile behavior when stress is applied. This versatility to be both stretched and compressed is more useful for cartilage tissue engineering as the purpose of the cartilage tissue is to allow for unhindered movement, which is not limited to only compression or only stretching (46, 47). Furthermore, the results of both tensile and compression tests show a general increase in the toughness of the hydrogels as the amount of alginate increases for both synthesis methods. This is to be expected as the high toughness and strength are derived from the brittle yet rigid sacrificial ionic alginate network. The unzipping of the ionic crosslinks supplies an energy dissipation mechanism; namely, the number of load-bearing polymer chains increases as the alginate network is unzipped (48, 49). The gels do however not completely break, during compression, due to the stretchable poly(AAM-co-AA) stabilizing the deformation once the ionic cross-links are broken (48, 49). Therefore, an increase in the relative amount of this rigid network will increase the overall rigidity and toughness of the DN hydrogel. However, this increasing trend which is coupled with the alginate content was not shown to be significant by the statistical analysis. The elastic moduli of the six formulations synthesized via the two- and one-step synthesis methods are only significantly different for a few select formulations (Figure 2 and Figure S1). In a similar fashion, the compressive moduli of the six formulations synthesized via the two- and one-step synthesis methods are also only significantly different for formulations 1A and 3A (Figure S3) synthesized via the one-step solution-gel method. The lack of significance is due to the high degree of variability in the modulus, which is also reflected by the maximum stress reached and might be attributed to the random nature of the radical copolymerization and cross-linking of the poly(AAM-co-AA) network (12). Furthermore, the carboxyl groups of the acrylic acid monomers can interact with the metal ions to create complex networks (32, 33). A study by Zhan et al. showed that radical copolymerized/crosslinked poly(AAM-co-AA) hydrogels can be crosslinked a second time via divalent or trivalent cations to change the mechanical properties (34). Therefore, the ionic crosslinking of the alginate network competes with the carboxyl groups introducing another level of randomness to the cross-linking. This phenomenon may also explain the generally slightly higher modulus and max stress obtained by the B variant of each formulation. As in these formulations, there are fewer carboxyl groups of acrylic acid present to disrupt the alginate network crosslinking.

Effect of the ionic crosslinker on the mechanical properties

Considering the previous results, it is decided that formulation 2A displays the best properties for cartilage tissue engineering. The versatility to display great toughness during compression combined with stretchability and equilibrium water content that approaches that of cartilage makes this formulation the preferred hydrogel. To further assess the mechanical properties the ionic crosslinking of the alginate network was further evaluated by the use of other cations (Mg^{2+}, Cu^{2+}, Fe^{2+}, Fe^{3+}, and Al^{3+}). The compressive properties of the differently crosslinked hydrogels were evaluated in compression tests at a strain speed of 1 mm/min until 90% strain was reached. All hydrogels reached 90% strain without major macroscopic damage occurring. The stress–strain curves and compressive modulus of all hydrogels are shown in Figure 4A & B. The average compressive moduli of the hydrogels crosslinked with Mg^{2+} and Cu^{2+} are similar to those crosslinked with Ca^{2+} (150 ± 72 kPa) at 100 ± 9 and 187 ± 28 kPa, respectively. The average max stress reached by these gels are also within the same order of magnitude as that of Ca^{2+} (2.15 ± 0.55 MPa) at 1.28 ± 0.54 MPa for Mg^{2+} and 7.56 ± 5.03 MPa for Cu^{2+}. The average compressive modulus of the hydrogels crosslinked with Fe^{2+} is considerably higher at 368 ± 18 MPa and the average max stress is correspondingly also high at

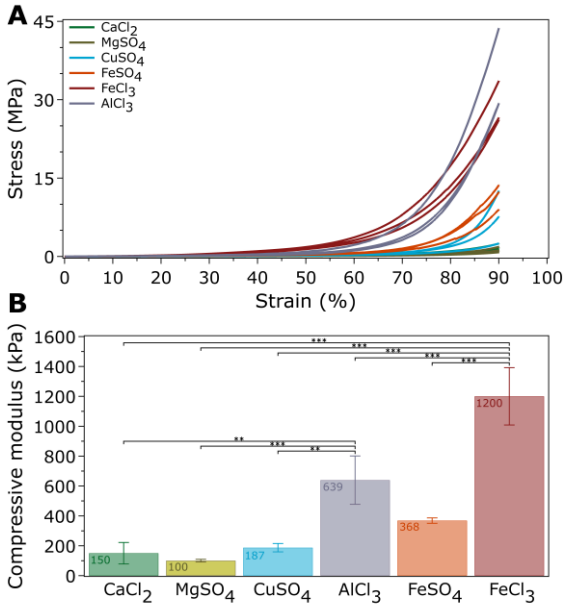

Figure 4 Compressive properties of DN hydrogels 2A crosslinked with various ions. All hydrogels display nonlinear viscoelastic behavior. **(A)** Compression stress-strain curves of the hydrogels. Crosslinking with Mg^{2+} and Cu^{2+} results in similar properties to crosslinking with Ca^{2+}. Crosslinking with Fe^{2+} considerably improves the properties. Crosslinking with the trivalent ions (Fe^{3+} & Al^{3+}) results in extremely tough hydrogels. **(B)** The compressive modulus of the hydrogels. Crosslinking with Mg^{2+} and Cu^{2+} results in a compressive modulus similar to that of Ca^{2+}. Crosslinking with Fe^{2+}, Fe^{3+}, and Al^{3+} considerably increases the modulus, however, only the differences in modulus for Fe^{3+} and Al^{3+} are significant as indicated.
** = P ≤ 0.01, *** = P ≤ 0.001

11.64 ± 2.41 MPa. Crosslinking with trivalent ions further raises these properties. The average compressive modulus of the hydrogels crosslinked with Al^{3+} is 639 ± 162 MPa and the average max stress is 34.10 ± 8.32 MPa. Crosslinking with Fe^{3+} results in even stronger properties with an average compressive modulus of 1200 ± 192 kPa and an average max stress of 28.77 ± 5.29 MPa. The moduli of these hydrogels crosslinked via the trivalent ions are also the only significantly different as indicated (Figure 4B). These results thus clearly show the potential for further toughening of the scaffold to be able to reach compressive moduli that rival the modulus of native cartilage (0.23-0.85 MPa) (5, 7). The mechanistic basis for these differences lies in the alginate chain folding, the local and global structures of alginate, and the nature of the interactions between the uronic acid units and the cross-linking ions. Several experimental and quantum chemical studies have provided insight into these mechanisms (48, 50-53). It has been found that alginates have a certain affinity for certain ions, which is based on molecular orbital interactions. Alkaline earth metals form ionic bonds with an affinity hierarchy that is correlated to the interaction energy and ionic radius: Sr^{2+} > Ca^{2+} > Mg^{2+} (50-52). Whereas bivalent transition and trivalent metal ions were found to form strong coordinate-covalent bonds with an affinity hierarchy correlated to interaction energy and ionic radius: Cu^{2+} > Co^{2+} > Zn^{2+} > Mn^{2+} & Fe^{3+} ≈ Cr^{3+} > Al^{3+} ≈ Ga^{3+} >>> Sc^{3+} > La^{3+}. These affinities and binding modes also correspond to the mechanical properties reported here. The increased mechanical properties of the trivalent metal ions to the bivalent transition metal ions to the alkaline earth metals match the reported affinities Fe^{3+} > Al^{3+} > Fe^{2+} > Cu^{2+} > Ca^{2+} > Mg^{2+} (51-53). Furthermore, the participation of carboxyl groups of the acrylic acid monomers further complicates the networks which results in the enhanced mechanical properties reported here. Despite the enhanced mechanical properties, the applicability of these metal ions for tissue engineering is debatable. Ions such as Al^{3+}, $Fe^{3+/2+}$, and Cu^{2+} are known to be cytotoxic. Aluminum's toxicity results from interactions with the cell membrane and it replaces Mg^{2+} and Fe^{3+} disturbing intercellular communication, cellular growth, and secretory functions. Iron can also be cytotoxic, despite its participation in certain biological functions. An excess of circulating unbound iron results in corrosive/acidic effects and the production of harmful radicals which can lead to DNA damage and lipid peroxidation (54). Copper's toxicity results from its oxidative potential, producing harmful radicals which can lead to lipid peroxidation. Furthermore, copper ions can non-specifically and irreversibly bind to thiol-containing proteins altering their activity (55).

Cyclical mechanical properties & energy dissipation

To further assess the mechanical properties of formulation 2A, cyclical compression tests were performed for 20 cycles with a downward strain speed of 5 mm/min and upward strain speed of 10 mm/min up to 90% strain. The stress–strain curves of the three replicates (cycles 1, 5, 10, 15, and 20) (Figure 5A), show that the gels effectively dissipate energy as shown by the pronounced hysteresis. An increase in the max stress is observed as the number of cycles increases, indicating stiffening of the scaffold as the strain keeps being reapplied. Furthermore, this data also clearly shows that a considerable decrease in absorbed energy occurs from the first cycle (27.7 ± 1.2 MJ/m^3) to the second (19.4 ± 1.4 MJ/m^3), indicating permanent damage occurring to the network. The energy then remains relatively constant at 19.1 ±1.5 MJ/m^3 from the second cycle onwards (Figure 5B). This level of energy dissipation is superior to those reported in the literature. Yang et al. reported hysteresis via tensile testing ranging from 588 to 2160 kJ/m^3 for alginate/polyacrylamide hydrogels crosslinked with various ions (48). The energy absorption is accompanied by an increase in the maximum stress reached. The maximum stress rises from 4.69 ± 0.59 MPa to 6.35 ± 0.64 MPa (Figure 5B), indicating a stiffening of the network as the strain keeps being reapplied beyond the first cycle. The intercycle strain stiffening of the scaffolds could result due to a variety of reasons. On a macroscopic level, water exudation during the cyclical compression and general drying of the hydrogel during the measurements result in a toughening of the hydrogels. On a microscopic level, the stiffening of the polymer network occurs via either of the two following mechanisms: nonlinear tension build-up of the active chains beyond the

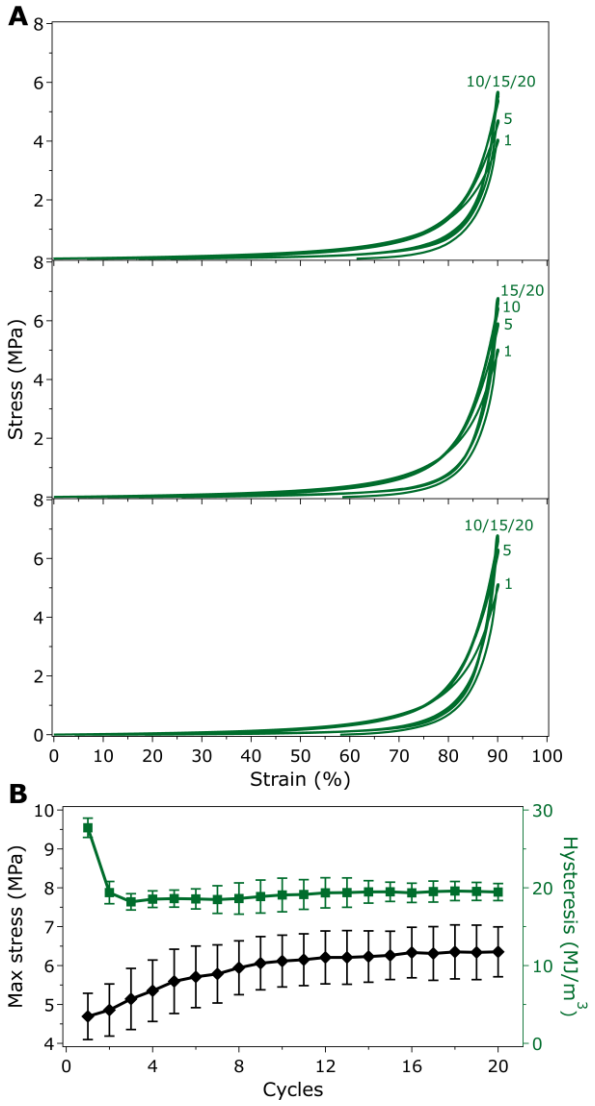

Figure 5 Cyclical mechanical properties & energy dissipation of hydrogel 2A. (A) Cyclical stress-strain curves of the three replicates (cycles 1, 5, 10, 15, 20). The hydrogels display viscoelastic behavior. The pronounced hysteresis shows the effective energy dissipation of the hydrogels during unloading. The max stress reached increases as the loading-unloading cycles continue. **(B)** Change in hysteresis (green) and max stress (black). The hysteresis of cycle one dissipates 27.7 MJ/m^3 of energy, which drastically drops to 19.4 MJ/m^3 of energy in cycle two. Indicating permanent network damage. However, no additional major damage occurs as the dissipated energy remains constant for the remaining cycles at 19.1 MJ/m^3. The max stress (black) steadily increases as the loading-unloading cycles continue, starting at 4.69 MPa and rising to 6.35 MPa. This phenomenon is known as strain stiffening and indicates a microscopic rearrangement of the network to increase deformation resistance.

Gaussian range (56-59) and deformation-induced reorganization of the network increasing the number of active chains (59-61). As stress is applied during the first cycle the ionic crosslinks of the alginate network are unzipped providing polymer chains to participate in load bearing. The poly(AAM-co-AA) also provides participating polymer chains. These participating polymer chains dissipate the initial energy and are microscopically altered (48, 49, 62). As stress is applied during the following cycle the remaining/recovered ionic crosslinks of the alginate network are further unzipped providing more participating polymer chains while the previously participating polymer chains continue building nonlinear tension (48, 49, 57). This continuous recruitment of active polymer chains while simultaneously building nonlinear tension results in a stiffening of the network (56-61). These macroscopic and microscopic mechanisms thus explain the increasing maximum stress, which starts plateauing from cycle 16 onward. This indicates that over time the amount of water exuded, and the number of participating polymer chains reaches a maximum and that the toughening of the scaffold is finite.

This resilient stiffening behavior is however promising for cartilage tissue engineering as, of course, during movement, the articular cartilage is continuously loaded and unloaded. This stiffening behavior is especially interesting when considering the extent of cartilage deformation. Several studies using advanced imaging techniques have shown that the deformation of the native cartilage tissue *in vivo* is limited to a compressive strain of ~10 % and max stress of 3.6 ± 1.3 MPa (46, 47, 63). The results thus indicate that the hydrogel scaffold reported here is capable of continuous cyclical deformation within a functional margin without breaking or deteriorating. Furthermore, the native cartilage tissue of the knee experiences both compression (superior-inferior) and shear (anterior-posterior) forces between the femur and tibia (46, 47, 63). The main purpose of the tissue is thus not to absorb energy through deformation but to effectively distribute the load equally to the subchondral bone plate and the muscles and tendons which will dissipate the energy (46, 47, 63). When considering these points, it can be said that the mechanical properties of the hydrogels reported here are sufficient for cartilage tissue engineering.

Alginate functionalization

Alginate purification

Alginate purification was performed to remove any contaminants or endotoxins present within the commercially available alginate before functionalization. The purification procedure did not alter the chemical structure of the sodium alginate as shown by GPC measurements and the FT-IR spectra. The FT-IR spectra (Figure S1A) are identical, indicating no alteration of the chemical structure due to the purification procedure. The broad O-H stretching band at 3570-3100 cm^{-1} can be identified as well as the COO asymmetric and symmetric stretching peaks at 1635 cm^{-1} and 1419 cm^{-1}, respectively. At 1050-1250 cm^{-1}, several peaks can be identified corresponding to C-O-C stretching. Furthermore, at 820 cm^{-1} and 946 cm^{-1}, the C-H stretching of the mannuronic acid and guluronic acid units, respectively, can be identified. Furthermore, the GPC data shows no significant change in de molecular weight distribution of the commercial alginate and purified alginate (Figure S1B). The molecular weight changes from 130 kg/mol to 127 kg/mol, which is a negligible difference ascribed to the standard variance in molecular weight of

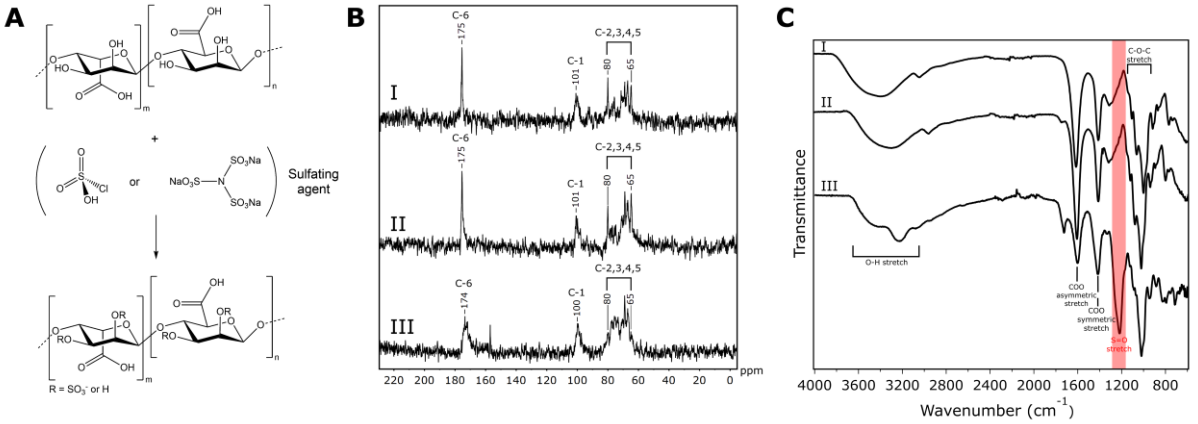

Figure 6 Characterization of the alginate sulfation reactions. (A) Sulfation reaction between alginate and chlorosulfonic acid or $N(SO_3Na)_3$ resulting in alginate sulfate with possible sulfate groups in the R positions attached to C-2,3. **(B)** The ^{13}C-NMR spectra of alginate (I), the reaction product of $N(SO_3Na)_3$ (II), and the reaction product of chlorosulfonic acid (III). All three spectra show the carbonyl carbon (C-6) at δ = 175/174 ppm, the anomeric carbon (C-1) at δ = 101/100 ppm, and the remaining carbon atoms (C-2,3,4,5) in the range δ = 80-65 ppm. Successful sulfation will result in a downward shift of C-2,3 and an upward shift of C-4,5. This is only noticeable for the reaction product of chlorosulfonic acid (III) as the intensity of the peaks within the δ = 80-65 ppm range is skewed toward 65 ppm, thereby indicating the downward shift of C-2,3 which are directly bonded to electronegative sulfate groups. However, due to incomplete sulfation normal signals for C-2,3,4,5 are also present diminishing the strength of the shift. **(C)** The FTIR spectra of alginate (I), the reaction product of $N(SO_3Na)_3$ (II), and the reaction product of chlorosulfonic acid (III). All spectra display the characteristic alginate peaks at 3570-3100 cm^{-1} (O-H), 1635 cm^{-1} and 1419 cm^{-1} (COO), 1050-1250 cm^{-1} (C-O-C). Only the reaction product of chlorosulfonic acid (III) also displays a characteristic sulfate peak at 1225 cm^{-1} (S=O) indicating successful sulfation via the reaction with chlorosulfonic acid.

polysaccharides. The dispersity (Đ) also changes slightly from 1.59 to 1.65. The element analysis also shows almost identical results. The commercial alginate contained 31% C, 4.3% H, and > 1% N & S, while the purified alginate contained 30% C, 4.2% H, and > 1% N & S. The overall yield of the procedure was ~87%, indicating that some product was lost during the centrifugation and filtration steps.

Alginate sulfation

Alginate sulfation was performed to introduce bioactive sulfate moieties onto the poly(AAM-co-AA)/alginate DN hydrogel. The sulfation of the natural polysaccharide alginate will mimic the natural function of the sulfated GAG chondroitin sulfate. Two sulfation methods are explored, the reaction with the conventional sulfating agent chlorosulfonic acid, and the unconventional sulfating agent $N(SO_3Na)_3$ (Figure 6A). The latter allows for the reaction to proceed in an aqueous environment thereby avoiding the possibility of partial depolymerization due to the acidic environment.

The sulfation reaction between alginate and chlorosulfonic acid was successful, as shown by both the ^{13}C-NMR and FTIR spectrum and the element analysis. The ^{13}C-NMR spectrum (Figure 6B) displays peaks corresponding to the carbonyl carbon (C-6) at δ = 175 and 174 ppm for the starting alginate (I) and the reaction product (III), respectively. The anomeric carbon (C-1) appears at δ = 101 and 100 ppm, respectively. The remaining carbon atoms (C-2,3,4,5) give peaks in the range δ = 80-65 ppm for both spectra. However, the intensity of the peaks in the δ = 80-65 ppm range is skewed towards the lower field position of 65 ppm for the reaction product (III). This indicates a shift of C-2,3 towards a lower field position, which is associated with a direct bond to electronegative sulfate groups (23, 24). However, due to incomplete sulfation normal signals for C-2,3,4,5 are also present diminishing the strength of the shift. Furthermore, the FTIR spectrum (Figure 6B) of the reaction product displays the characteristic peaks of alginate at 3570-3100 cm^{-1} (O-H), 1635 cm^{-1} and 1419 cm^{-1} (COO), 1050-1250 cm^{-1} (C-O-C), 820 cm^{-1} and 946 cm^{-1} (C-H). In addition to these peaks, a characteristic sulfate peak is also present at 1225 cm^{-1} (S=O), thereby confirming the addition of sulfate moieties. The element analysis also supports this conclusion as the reaction product contains 9.56% sulfur indicating a DS of 0.85. Meaning that of the two hydroxyl groups that each monomer contains, on average, 0.85 are replaced by sulfate groups. This gives a total conversion of 42.5 %. All these characterization results support each other and show that the sulfation reaction between alginate and chlorosulfonic acid was successful.

Despite the success of the functionalization reaction, the DS is considerably lower than expected. Ronghua et al. reported a DS of 1.41 for the reaction with 20 vol% chlorosulfonic acid (23). Lower DS are reported in the literature for the reaction with chlorosulfonic acid, however, the vol% used is also much lower. Baei et al. reports a DS of 0.45 and 0.67 for the reaction with 2 and 3 vol% chlorosulfonic acid (22). Daemi et al. reports a DS of 0.9 for the reaction with 3.5 vol% chlorosulfonic acid (64). The DS reported here is thus more in line with the reactions using 2 - 3.5 vol% of chlorosulfonic acid. This discrepancy might be explained by the presence of water in the reaction setup, as chlorosulfonic acid is known to violently react with water to yield sulfuric acid and hydrogen chloride. When the chlorosulfonic acid was added, a considerable amount of vapor formed indicating the formation of HCl and thus the presence of water. This reaction might have decreased the remaining chlorosulfonic acid, resulting in an actual concentration available for the reaction with alginate at 2 - 3.5 vol%.

The sulfation reaction between alginate and $N(SO_3Na)_3$ was unsuccessful as shown by both the ^{13}C-NMR, FTIR spectrum, and the element analysis. The ^{13}C-NMR spectrum (Figure 6B) of the reaction product (II) was identical to the spectrum of the starting alginate (I). Peaks corresponding to the carbonyl carbon (C-6) appeared in both spectra at δ = 175 ppm for the starting alginate and the reaction product. The anomeric carbon (C-1) appeared in both spectra at δ = 101 ppm. The remaining carbon atoms (C-2,3,4,5) give peaks in the range δ = 80-65 ppm for both spectra. If the sulfation was successful, a downward shift of C-2,3 would be expected as these would be directly bound to electronegative sulfate ester groups while an upward shift of C-4,5 would be expected as these would be indirectly bonded to sulfate ester groups (24). Therefore, based on this result, the sulfation could not be confirmed. Furthermore, the FTIR spectrum (Figure 6C) of the reaction product was identical to the spectrum of the starting alginate. The typical peaks corresponding to the functional groups of standard alginate could be identified at 3570-3100 cm^{-1} (O-H), 1635 cm^{-1} and 1419 cm^{-1} (COO), and 1050-1250 cm^{-1} (C-O-C). The expected peak associated with a sulfate group at ~1250 cm^{-1} did not appear in the spectrum of the reaction product (II) (23, 24). This result once again indicates that the sulfation reaction was unsuccessful. The element analysis also supports this conclusion as the reaction product contain > 1 % sulfur indicating a DS > 0.06, while the expected DS was ~1.4-1.9 as reported by Fan et al. (24). All these characterization result support each other and show that the sulfation reaction between alginate and $N(SO_3Na)_3$ was unsuccessful.

Several parameters of the reaction greatly impact the DS. First of all the sulfating agent $N(SO_3Na)_3$ is only moderately reactive and activity might further decrease when the $-SO_3Na$ groups are reduced forming $HN(SO_3Na)_2$ (24). Secondly, the pH of the sulfation medium is important due to alkaline conditions deprotonating the alginate's hydroxyl groups, which is favorable for the reaction with the sulfating agent. Therefore, when the pH is too low or too high the formed alginate sulfate might be hydrolyzed removing the sulfate group (24). Therefore, the adjustment of the reaction medium to 9 and the neutralization after the completion of the reaction might have been performed incorrectly and affected the sulfation as the pH was monitored with indicator strips instead of a pH meter. The temperature of the reaction also greatly affects the DS, with 40 °C being the optimal temperature (24). The viscosity of the solution might impair the stirring, resulting in an inhomogeneous and sub-optimal heat transfer through the reaction medium. This may also impact the time required to allow the reaction to proceed to completion. The optimal time was 4 h, after which the DS would remain constant (24). However, in sub-optimal reaction conditions, incorrect pH, and impaired heat transfer, the required time may be longer than 4 h.

Poly(AAM-co-AA)/alginate sulfate DN hydrogel

Mechanical properties

The previous evaluation of the mechanical properties of the non-bioactive poly(AAM-co-AA)/alginate DN hydrogel has shown that formulation 2A displays the best properties for cartilage tissue engineering. The versatility to display great toughness during compression combined with stretchability and an equilibrium water content that approaches that of cartilage makes this formulation the preferred hydrogel formulation. Therefore, this formulation was used to assess the effect of the sulfation on the mechanical properties of the DN hydrogels. The mechanical properties of these bioactive hydrogels were evaluated in both tensile and compression tests. The tensile and compressive stress–strain curves show the nonlinear viscoelastic behavior of the tough hydrogels (Figure 7A & C). Following the application of strain, elastic deformation occurs up to ~50-75% strain. As the strain further increases, stress relaxation occurs due to the disruption of ionic and transient physical cross-links, enabling the rearrangement of the network. This is predominantly facilitated by water migration and exudation (35, 36). The Young's modulus of each hydrogel was determined within the elastic deformation region, specifically 10-20 % strain.

The tensile tests were performed at a strain speed of 50 mm/min until gel rupture of the bioactive formulation 2A, synthesized via the one-step solution-gel method. The stress–strain curves and elastic modulus are shown in Figure 7A & B. The sulfated DN hydrogels reach an average elastic modulus of 74.9 ± 28 kPa, which is decreased compared to the normal DN hydrogels, which reached a modulus of 96.6 ± 14 kPa (Figure 7B). This is a decrease of 22.5%, which could be explained due to electrostatic repulsion and steric hindrance. The negatively charged sulfate groups may electrostatically repulse the alginate chains, thereby preventing ionic crosslinking. Additionally, the large sulfate moieties on the chains may prevent cross-linking via steric hindrance (20, 22). However, the statistical analysis shows that this decrease is not significant (p-value = 0.32) enough to truly indicate that the sulfated hydrogels behave mechanically different. The DS is most likely not high enough for these electrostatic and steric effects to make a significant difference in the crosslinking of the alginate network (20, 22). The difference in moduli is most likely the product of the general variability of the hydrogels which was also observed for the six different non-bioactive hydrogels formulations. Conversely, there is a noticeable decrease in the ductility of the gels as the most ductile sulfate hydrogel could reach a maximum strain of ~687% compared to the maximum strain of ~1320% for the normal hydrogels (Figure 7A). This decrease in ductility, although noticeable, does not impact the applicability of the sulfated hydrogels for tissue engineering. Extensibility of 6.9 times its length is still superior to that of articular cartilage (up to 1.4 times) (5). These elastic properties are also superior to other hydrogel systems mimicking the function of chondroitin sulfate. Fenbo et al. reports a loss modulus G', which reflects the elastic properties, of ~30 kPa for an alginate/chondroitin sulfate hybrid hydrogel (65). Shah et al. reports a loss modulus G' of ~4.8 kPa for a chondroitin sulfate grafted alginate-Poloxamer-407

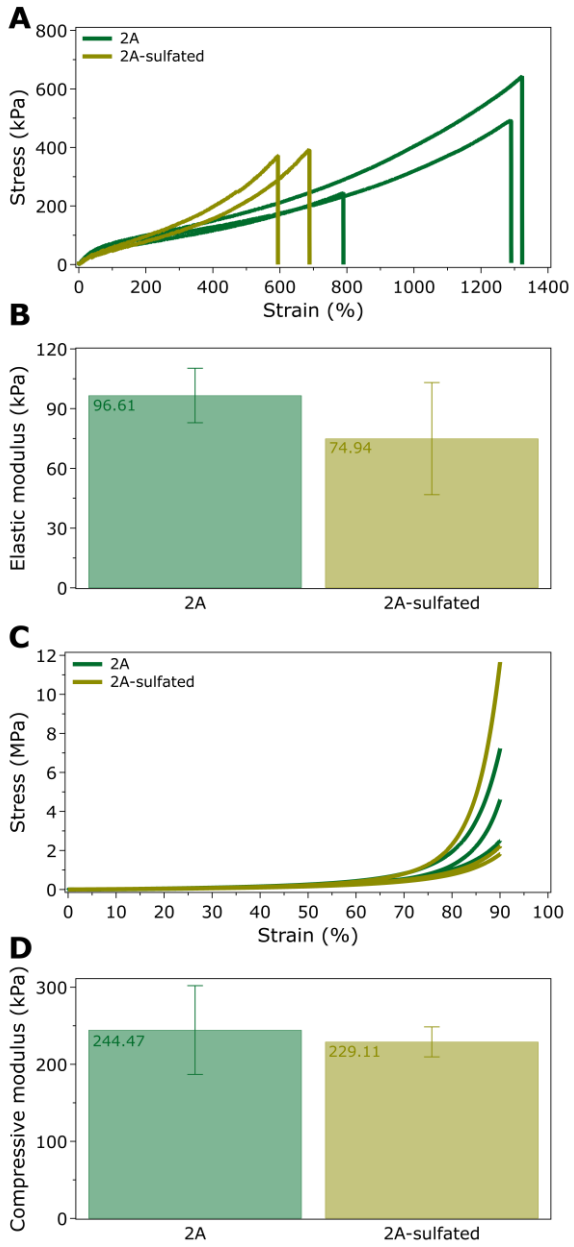

Figure 7 Mechanical properties of the bioactive DN hydrogel 2A. All hydrogels display nonlinear viscoelastic behavior. **(A)** Tensile stress-strain curves of the sulfated and non-sulfated hydrogel formulation 2A. A clear decrease in ductility is apparent for the sulfated hydrogels. **(B)** Elastic modulus of the sulfated and non-sulfated hydrogel formulation 2A. The elastic properties of the sulfated hydrogels are diminished compared to the non-sulfated hydrogels. However, statistical analysis indicates that there is no significant difference. **(C)** Compressive stress-strain curves of the sulfated and non-sulfated hydrogel formulation 2A. The sulfated hydrogels display properties in line with the non-sulfated hydrogels. **(D)** Compressive modulus of the sulfated and non-sulfated hydrogel formulation 2A. The compressive toughness of the sulfated and non-sulfated hydrogels were not significantly different.

(F127) hybrid hydrogel (66). Zare et al. reports elastic moduli ranging from 4.91-24.21 kPa for a KNG-loaded poly(lactic-co-glycolic acid) nanoparticle impregnated alginate/alginate sulfate polycaprolactone nanofiber composite hydrogel (67).

The compressive properties of the bioactive hydrogel were evaluated in compression tests at a strain speed of 1 mm/min until 90 % strain is reached. All three replicates reached 90 % strain without major macroscopic damage occurring. The stress–strain curves and compressive modulus are shown in Figure 7C & D. The sulfated DN hydrogels reach an average compressive modulus of 229 ± 19 kPa which is slightly decreased compared to the normal DN hydrogels which reached a modulus of 244 ± 58 kPa; this is a 6.2% decrease. Despite this slight decrease, the modulus lies within the compressive modulus of native cartilage (0.23-0.85 MPa) (5, 7). This decrease could, once again, be attributed to the due to electrostatic repulsion and steric hindrance of the sulfate groups (20, 22). However, as with the tensile test, the statistical analysis indicates that this decrease is not significant (p-value = 0.68). The DS is most likely not high enough for the sulfate groups to have a pronounced effect on the crosslinking and this decrease should be considered the result of the general variability of the hydrogels. The average maximum stress reached by the bioactive hydrogels is 5.23 ± 5.6 MPa, which is higher than the average maximum stress of the non-sulfated hydrogels (4.77 ± 2.4 MPa). This increase is most likely due to one outlier gel which reached a maximum stress of 11.7 MPa. When disregarding this replicate the average maximum stress becomes 2.01 ± 0.28 MPa, which is lower than the non-sulfated hydrogel. This variability of the average maximum stress is in line with the variability observed earlier for the six different hydrogel formulations. Thus, once again, these changes cannot be solely contributed to the electrostatic and steric effect of the sulfate groups. These compressive properties are also superior to other hydrogel systems mimicking the function of chondroitin sulfate. The KNG-loaded poly(lactic-co-glycolic acid) nanoparticle-impregnated alginate/alginate sulfate polycaprolactone nanofiber composite hydrogel reported by Zare et al. reached a maximum stress of 6-15 kPa (67). Mhanna et al. report a compressive modulus of 2.4 ± 0.57 kPa for a pure alginate sulfate hydrogel (20). Goto et al. report a compressive modulus of 22.5 ± 6.3 kPa for a phenol-grafted alginate sulfate hydrogel (68). These reported results clearly show the benefits of the double network formulation.

When the results of both the tensile and compression tests are analyzed together, it can be concluded that the sulfation results in a slight decrease of the elastic and compressive properties, which is not significant. Ductility is the only mechanical parameter that noticeably decreased. Overall, it can be stated that the sulfated hydrogels with an alginate DS of 0.85 do not alter the mechanical properties. A greater decrease in the properties is expected for alginate with a higher DS as the electrostatic and steric effects will become more pronounced and thus affect the ionic crosslinking (20, 22). It can be concluded that the sulfated DN hydrogel reported here is promising for cartilage tissue engineering as it combines acceptable ductility with good compressive properties. However, the compressive properties should be further enhanced to elevate the properties closer to the desired range of 0.23-0.85 MPa (5, 7). This could be achieved via

crosslinking with Al^{3+} or Fe^{3+} as demonstrated before with the non-sulfated hydrogels. It can be reasoned that the sulfated hydrogels will display a similar increase in properties due to the cross-linking with trivalent ions as the non-sulfated hydrogel since the crosslinking with Ca^{2+} gave similar properties. Increasing the alginate G-block content could also result in increased properties to avoid the possible toxicity of other ions besides Ca^{2+}.

Cyclical mechanical properties & energy dissipation

To further assess the effect of the sulfation on the mechanical properties, cyclical compression tests were performed for 20 cycles with a downward strain speed of 5 mm/min and upward strain speed of 10 mm/min up to 90 % strain. The stress–strain curves of the three replicates (cycle 20) (Figure 8A) show that the gels effectively dissipate energy like the non-sulfated hydrogels. However, unlike the non-sulfated hydrogels, no pronounced strain stiffening behavior or drastic decrease in absorbed energy is observed (Figure 8B). The energy dissipation of the sulfated hydrogels is altered since no significant drop in energy dissipation from cycles 1 to 2 is observed. The hysteresis changes from 17.6 to 15.5 MJ/m^3 when going from cycles 1 to 2 (Figure 8B). This is only a drop of 2.1 MJ/m^3 compared to the 8.3 MJ/m^3 drop for the non-sulfated hydrogels. This seems to indicate that the sulfated hydrogel scaffold is not permanently damaged, or only damaged to a lesser extent when compared to the non-sulfated hydrogels. The dissipated energy remains relatively constant over all 20 cycles at ~15.7 ± 3.6 MJ/m^3 (Figure 8B), which is similar to the 19.1 ±1.5 MJ/m^3 constant of the non-sulfated hydrogels. The energy dissipation displayed here is also higher than in other hydrogel systems. The KNG-loaded poly(lactic-co-glycolic acid) nanoparticle-impregnated alginate/alginate sulfate polycaprolactone nanofiber composite hydrogel reported by Zare et al. had a toughness of 2235 J/m^3 (67). Yang et al. reported hysteresis via tensile testing ranging from 588 to 2160 KJ/m^3 for alginate/polyacrylamide hydrogels crosslinked with various ions (48). The constant energy dissipation is also accompanied by a relatively constant maximum stress. The maximum stress rises slightly from 4.03 ± 0.98 to 4.29 ± 0.85 MPa at cycle 17, and then slightly decreases again to 4.23 ± 0.79 MPa at cycle 20 (Figure 8B). This change in maximum stress is negligible, compared to the max stress increase for the normal hydrogels (1.45 MPa). Hence, the sulfated hydrogels do not seem to display the same intercycle strain stiffening behavior as their non-sulfated counterpart. The reason behind this change in behavior might be due to the macroscopic water exudation effect which is at the basis of the strain stiffening behavior of the non-sulfated hydrogels. Sulfates are one of the most hydrophilic anions and are notoriously difficult to dehydrate (69). Therefore, the continuous loading and unloading of the hydrogel might not have greatly dried the hydrogel due to the presence of the strongly hydrophilic sulfate anions (69). Despite the absence of this stiffening behavior, they do exhibit the same resilient behavior under cyclical loading and unloading as the max stress remains constant.

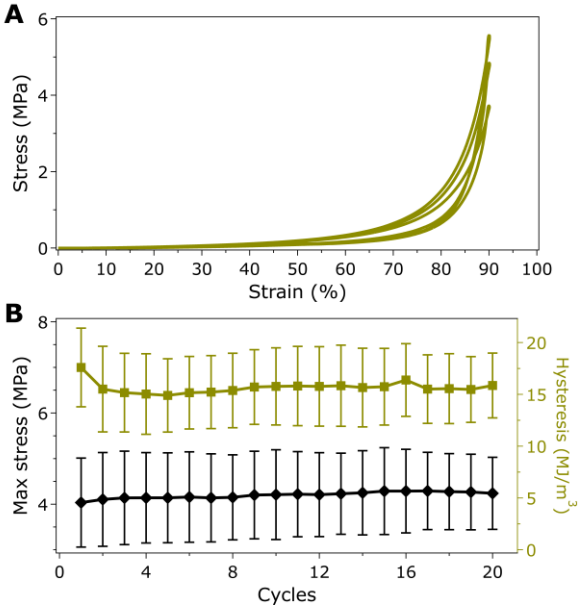

Figure 8 Cyclical mechanical properties & energy dissipation of bioactive DN hydrogel 2A. (A) Cyclical stress-strain curves of the three replicates (cycle 20). The hydrogels display viscoelastic behavior. The pronounced hysteresis shows the effective energy dissipation of the hydrogels during unloading. **(B)** Change in hysteresis (olive green) and max stress (black). The hysteresis remains relatively constant throughout the 20 loading-unloading cycles at 15.7 ± 3.6 MJ/m^3. A slight drop of 2.1 MJ/m^3 from 17.6 to 15.5 MJ/m^3 is observed when going from cycle 1 to 2. This indicates that minimal network damage occurs through cyclical deformation. The max stress (black) also remains relatively constant at 4.20 ± 0.07 MPa as the loading-unloading cycles continue showing the remarkable resilience of the DN hydrogels under continuous deformation.

In conclusion, it is apparent that the sulfated hydrogel resilience during cyclical loading and unloading is extremely promising for cartilage tissue engineering. Especially since the loading and unloading were done up to 90% strain each cycle. This is well above the functional range of *in vivo* cartilage deformation (~10 % stain) as the main purpose of the tissue is not deformation and energy absorption but rather load distribution and conduction (46, 47, 63).

■ CONCLUSION AND FUTURE OUTLOOK

This research reports on the synthesis and biofunctionalization of poly(acrylamide-co-acrylic acid)/alginate DN hydrogels. The results showed that the hydrogel synthesis method employed, and the hydrogel formulation chosen can greatly affect the obtained mechanical properties. The results showed that a one-step *in situ* crosslinking method which crosslinks both networks simultaneously results in hydrogels with superior properties when compared to a two-step sequential crosslinking method. Furthermore, the results clearly show rising trends in stiffness coupled to the wt% of the rigid densely crosslinked alginate network. This increase in elastic stiffness is conversely also tied to a decreasing trend in ductility. The compressive properties also show rising trends in stiffness coupled to the wt% of the rigid densely

crosslinked alginate network. It was found that a formulation using 2 wt% alginate results in the most well-rounded properties which combine both high compressive and elastic stiffness with considerable ductility. The composition of the second network showed no great influence on the mechanical properties. An 80:20 or 90:10 ratio of acrylamide:acrylic acid monomers did not greatly affect the mechanical properties. Therefore, a higher amount of acrylic acids was chosen as the most optimal formulation given future biofunctionalization possibilities via the carboxylic acid groups present. The compressive mechanical properties of this optimal formulation were within the range of the targeted articular cartilage (0.23-0.8 MPa) (5, 7). This optimal formulation also displayed strain stiffening behavior in cyclical loading-unloading experiments, clearly showing great promise for articular cartilage tissue engineering. Although these properties are already formidable further enhancement of the properties should still be pursued. This work therefore also explored the possibilities to further enhance the properties via ionic crosslinking through various divalent and trivalent ions. The results showed that crosslinking with Al^{3+} or Fe^{3+} could seriously enhance the properties to reach compressive moduli of 1 MPa. However, concerns about cytotoxicity limit the applicability of this strengthening route. Further research should therefore focus on the enhancement of the mechanical properties via biocompatible mechanisms. The most straightforward alternative is using alginates with an increased G-block content, thereby increasing the number of ionic crosslinks. Another interesting way to strengthen hydrogel properties is via nanocomposite formulations using nanoparticles. Bioactive nanoparticles could be implemented to enhance the crosslinking density and impart some added degree of bifunctionality (70, 71).

Besides mechanical properties, this work also ventured into the biofunctionalization of these hydrogels through the sulfation of the alginate network. This sulfation would mimic the functions of chondroitin sulfate, a crucial component in the development, and maintenance of tissues by serving as (co-)receptors and reservoirs of growth factors through electrostatic interaction (17, 20, 21, 22). The sulfation was successful via the reaction with chlorosulfonic acid resulting in a DS of 0.85. The introduction of this sulfate group did not drastically alter the mechanical properties of the hydrogels. Only a decrease in ductility was noticeable. Nevertheless, the mechanical properties were still suitable for cartilage tissue engineering since the sulfated hydrogels also displayed impressive resilience in cyclical compression tests. Assessing the bioactivity of these hydrogels was outside of the scope of this work. However, further analysis of the sulfated hydrogels is required. Past studies have shown that sulfated hydrogel scaffolds can effectively sequester and slowly release growth factors such as TGF-β1 (22). Studying the retention and release profile of growth factors from the DN hydrogels reported here is therefore a logical next step in the research. Further enhancing the bioactivity via other strategies should also be pursued. Elastin-like polypeptides (ELPs) are an attractive biofunctional handle to be introduced as well, due to their genetically modifiable nature. This allows for the possibility to introduce an arginyl-glycyl-aspartic acid (RGD) cell adhesion domain and a guest residue for chemical attachment to the hydrogel building blocks (72-75). These RGD-ELPs could be conjugated to either the alginate or poly(acrylamide-co-acrylic acid) network via the ε-amine of lysine residues of peptides and proteins which can be readily linked to an activated carboxylic acid to form an amide bond using carbodiimide chemistry (74).

To summarize, this work provides the basic fundamental insights required to further enhance the mechanical and bioactive properties of the proposed poly(acrylamide-co-acrylic acid)/alginate sulfate DN hydrogel system. Further enhancement of these properties could establish a basis for extensive *in vitro* cell testing which brings the field closer to an applicable tissue engineering treatment for osteoarthritis.

■ REFERENCES

1. Ahmed EM. Hydrogel: Preparation, characterization, and applications: A review. J Adv Res. 2015;6(2):105-21.
2. Aswathy SH, Narendrakumar U, Manjubala I. Commercial hydrogels for biomedical applications. Heliyon. 2020;6(4):e03719.
3. Mantha S, Pillai S, Khayambashi P, Upadhyay A, Zhang Y, Tao O, et al. Smart Hydrogels in Tissue Engineering and Regenerative Medicine. Materials (Basel). 2019;12(20).
4. Li X, Sun Q, Li Q, Kawazoe N, Chen G. Functional Hydrogels With Tunable Structures and Properties for Tissue Engineering Applications. Front Chem. 2018;6:499.
5. Hafezi M, Nouri Khorasani S, Zare M, Esmaeely Neisiany R, Davoodi P. Advanced Hydrogels for Cartilage Tissue Engineering: Recent Progress and Future Directions. Polymers (Basel). 2021;13(23).
6. Zhou L, Guo P, D'Este M, Tong W, Xu J, Yao H, et al. Functionalized Hydrogels for Articular Cartilage Tissue Engineering. Engineering. 2022;13:71-90.
7. Korhonen RK, Laasanen MS, Töyräs J, Rieppo J, Hirvonen J, Helminen HJ, et al. Comparison of the equilibrium response of articular cartilage in unconfined compression, confined compression, and indentation. Journal of Biomechanics. 2002;35(7):903-9.
8. Chen Q, Chen H, Zhu L, Zheng J. Fundamentals of Double Network Hydrogels. J Mater Chem B. 2015;3.
9. Huang X, Li J, Luo J, Gao Q, Mao A, Li J. Research progress on double-network hydrogels. Materials Today Communications. 2021;29:102757.
10. Spicer CD. Hydrogel scaffolds for tissue engineering: the importance of polymer choice. Polymer Chemistry. 2020;11(2):184-219.
11. Tonbul M, Adas M, Bekmezci T, Kara AD. Intra-articular polyacrylamide hydrogel injections are not innocent. Case Rep Orthop. 2014;2014:150709.
12. Sennakesavan G, Mostakhdemin M, Dkhar LK, Seyfoddin A, Fatihhi SJ. Acrylic acid/acrylamide based hydrogels and its properties - A review. Polymer Degradation and Stability. 2020;180:109308.

13. Sun J-Y, Zhao X, Illeperuma WRK, Chaudhuri O, Oh KH, Mooney DJ, et al. Highly stretchable and tough hydrogels. Nature. 2012;489(7414):133-6.
14. Liu W, Madry H, Cucchiarini M. Application of Alginate Hydrogels for Next-Generation Articular Cartilage Regeneration. Int J Mol Sci. 2022;23(3).
15. Smidsrød O, Skjåk-Braek G. Alginate as immobilization matrix for cells. Trends Biotechnol. 1990;8(3):71-8.
16. Vyas C, Mishbak H, Cooper G, Peach C, Pereira RF, Bartolo P. Biological perspectives and current biofabrication strategies in osteochondral tissue engineering. Biomanufacturing Reviews. 2020;5(1):2.
17. Klecker C, Nair LS. Chapter 13 - Matrix Chemistry Controlling Stem Cell Behavior. In: Vishwakarma A, Karp JM, editors. Biology and Engineering of Stem Cell Niches. Boston: Academic Press; 2017. p. 195-213.
18. Henrotin Y, Mathy M, Sanchez C, Lambert C. Chondroitin sulfate in the treatment of osteoarthritis: from in vitro studies to clinical recommendations. Ther Adv Musculoskelet Dis. 2010;2(6):335-48.
19. Baeurle SA, Kiselev MG, Makarova ES, Nogovitsin EA. Effect of the counterion behavior on the frictional–compressive properties of chondroitin sulfate solutions. Polymer. 2009;50(7):1805-13.
20. Mhanna R, Kashyap A, Palazzolo G, Vallmajo-Martin Q, Becher J, Möller S, et al. Chondrocyte Culture in Three Dimensional Alginate Sulfate Hydrogels Promotes Proliferation While Maintaining Expression of Chondrogenic Markers. Tissue Engineering Part A. 2013;20(9-10):1454-64.
21. Arlov Ø, Skjåk-Bræk G. Sulfated Alginates as Heparin Analogues: A Review of Chemical and Functional Properties. Molecules. 2017;22:778.
22. Baei P, Daemi H, Mostafaei F, Azam Sayahpour F, Baharvand H, Baghaban Eslaminejad M. A tough polysaccharide-based cell-laden double-network hydrogel promotes articular cartilage tissue regeneration in rabbits. Chemical Engineering Journal. 2021;418:129277.
23. Ronghua H, Yumin D, Jianhong Y. Preparation and in vitro anticoagulant activities of alginate sulfate and its quaterized derivatives. Carbohydrate Polymers. 2003;52(1):19-24.
24. Fan L, Jiang L, Xu Y, Zhou Y, Shen Y, Xie W, et al. Synthesis and anticoagulant activity of sodium alginate sulfates. Carbohydrate Polymers. 2011;83(4):1797-803.
25. Lim D-W, Whang HS, Yoon K-J, Ko S-W. Synthesis and absorbency of a superabsorbent from sodium starch sulfate-g-polyacrylonitrile. Journal of Applied Polymer Science. 2001;79(8):1423-30.
26. Lowman A. Smart Pharmaceuticals. 2023.
27. Ganji F, Vasheghani Farahani S, Vasheghani-Farahani E. Theoretical Description of Hydrogel Swelling: A Review. Iranian Polymer Journal. 2010;19:375-98.
28. Bajpai S. Swelling studies on hydrogel networks - A review. Journal of Scientific and Industrial Research. 2001;60:451-62.
29. Erceg T, Cakić S, Cvetinov M, Dapčević-Hadnađev T, Budinski-Simendić J, Ristić I. The properties of conventionally and microwave synthesized poly(acrylamide-co-acrylic acid) hydrogels. Polymer Bulletin. 2020;77(4):2089-110.
30. Erceg T, Dapčević-Hadnađev T, Hadnađev M, Ristić I. Swelling kinetics and rheological behaviour of microwave synthesized poly(acrylamide-co-acrylic acid) hydrogels. Colloid and Polymer Science. 2021;299(1):11-23.
31. Kim D, Park K. Swelling and mechanical properties of superporous hydrogels of poly(acrylamide-co-acrylic acid)/polyethylenimine interpenetrating polymer networks. Polymer. 2004;45(1):189-96.
32. Kolya H, Roy A, Tripathy T. Starch-g-Poly-(N, N-dimethyl acrylamide-co-acrylic acid): An efficient Cr (VI) ion binder. International Journal of Biological Macromolecules. 2015;72:560-8.
33. Kolya H, Das S, Tripathy T. Synthesis of Starch-g-Poly-(N-methylacrylamide-co-acrylic acid) and its application for the removal of mercury (II) from aqueous solution by adsorption. European Polymer Journal. 2014;58:1-10.
34. Zhang H, Cheng Y, Hou X, Yang B, Guo F. Ionic effects on the mechanical and swelling properties of a poly(acrylic acid/acrylamide) double crosslinking hydrogel. New Journal of Chemistry. 2018;42(11):9151-8.
35. Zhao X, Huebsch N, Mooney DJ, Suo Z. Stress-relaxation behavior in gels with ionic and covalent crosslinks. J Appl Phys. 2010;107(6):63509.
36. Chen X, Dong C, Wei K, Yao Y, Feng Q, Zhang K, et al. Supramolecular hydrogels cross-linked by preassembled host–guest PEG cross-linkers resist excessive, ultrafast, and non-resting cyclic compression. NPG Asia Materials. 2018;10(8):788-99.
37. Guo P, Yuan Y, Chi F. Biomimetic alginate/polyacrylamide porous scaffold supports human mesenchymal stem cell proliferation and chondrogenesis. Mater Sci Eng C Mater Biol Appl. 2014;42:622-8.
38. Yi J, Nguyen K-CT, Wang W, Yang W, Pan M, Lou E, et al. Polyacrylamide/Alginate double-network tough hydrogels for intraoral ultrasound imaging. Journal of Colloid and Interface Science. 2020;578:598-607.
39. Xu C, Zhang X, Liu S, Zhao X, Geng C, Wang L, et al. Selected Phase Separation Renders High Strength and Toughness to Polyacrylamide/Alginate Hydrogels with Large-Scale Cross-Linking Zones. ACS Applied Materials & Interfaces. 2021;13(21):25383-91.
40. Li J, Illeperuma WRK, Suo Z, Vlassak JJ. Hybrid Hydrogels with Extremely High Stiffness and Toughness. ACS Macro Letters. 2014;3(6):520-3.
41. Wang J, Wei J, Su S, Qiu J, Wang S. Ion-linked double-network hydrogel with high toughness and stiffness. Journal of Materials Science. 2015;50(16):5458-65.
42. Arjmandi M, Ramezani M. Mechanical and tribological assessment of silica nanoparticle-alginate-polyacrylamide nanocomposite hydrogels as a cartilage replacement. Journal of the Mechanical Behavior of Biomedical Materials. 2019;95:196-204.
43. Cao Z, Zhang Y, Luo K, Wu Y, Gao H, Cheng J, et al. Preparation and Properties of Polyacrylamide/Sodium Alginate Hydrogel and the Effect of Fe Adsorption on Its Mechanical Performance. Journal of Renewable Materials. 2021;9:1447-62.
44. Chen Z, Tang J, Zhang N, Chen Y, Chen Y, Li H, et al. Dual-network sodium alginate/polyacrylamide/laponite nanocomposite hydrogels with high toughness and cyclic mechano-

responsiveness. Colloids and Surfaces A: Physicochemical and Engineering Aspects. 2022;633:127867.
45. Patel JM, Wise BC, Bonnevie ED, Mauck RL. A Systematic Review and Guide to Mechanical Testing for Articular Cartilage Tissue Engineering. Tissue Eng Part C Methods. 2019;25(10):593-608.
46. Chan DD, Cai L, Butz KD, Trippel SB, Nauman EA, Neu CP. In vivo articular cartilage deformation: noninvasive quantification of intratissue strain during joint contact in the human knee. Scientific Reports. 2016;6(1):19220.
47. Abusara Z, Von Kossel M, Herzog W. In Vivo Dynamic Deformation of Articular Cartilage in Intact Joints Loaded by Controlled Muscular Contractions. PLoS One. 2016;11(1):e0147547.
48. Yang CH, Wang MX, Haider H, Yang JH, Sun J-Y, Chen YM, et al. Strengthening Alginate/Polyacrylamide Hydrogels Using Various Multivalent Cations. ACS Applied Materials & Interfaces. 2013;5(21):10418-22.
49. Wang MX, Yang CH, Liu ZQ, Zhou J, Xu F, Suo Z, et al. Tough photoluminescent hydrogels doped with lanthanide. Macromol Rapid Commun. 2015;36(5):465-71.
50. Cozzi D, Desideri PG, Lepri L. The mechanism of ion exchange with algenic acid. Journal of Chromatography A. 1969;40:130-7.
51. Brus J, Urbanova M, Czernek J, Pavelkova M, Kubova K, Vyslouzil J, et al. Structure and Dynamics of Alginate Gels Cross-Linked by Polyvalent Ions Probed via Solid State NMR Spectroscopy. Biomacromolecules. 2017;18(8):2478-88.
52. Agulhon P, Markova V, Robitzer M, Quignard F, Mineva T. Structure of Alginate Gels: Interaction of Diuronate Units with Divalent Cations from Density Functional Calculations. Biomacromolecules. 2012;13(6):1899-907.
53. Menakbi C, Quignard F, Mineva T. Complexation of Trivalent Metal Cations to Mannuronate Type Alginate Models from a Density Functional Study. The Journal of Physical Chemistry B. 2016;120(15):3615-23.
54. Jaishankar M, Tseten T, Anbalagan N, Mathew BB, Beeregowda KN. Toxicity, mechanism and health effects of some heavy metals. Interdiscip Toxicol. 2014;7(2):60-72.
55. Letelier ME, Sánchez-Jofré S, Peredo-Silva L, Cortés-Troncoso J, Aracena-Parks P. Mechanisms underlying iron and copper ions toxicity in biological systems: Pro-oxidant activity and protein-binding effects. Chemico-Biological Interactions. 2010;188(1):220-7.
56. Séréro Y, Jacobsen V, Berret JF, May R. Evidence of Nonlinear Chain Stretching in the Rheology of Transient Networks. Macromolecules. 2000;33(5):1841-7.
57. Marrucci G, Bhargava S, Cooper SL. Models of shear-thickening behavior in physically crosslinked networks. Macromolecules. 1993;26(24):6483-8.
58. Ma SX, Cooper SL. Shear Thickening in Aqueous Solutions of Hydrocarbon End-Capped Poly(ethylene oxide). Macromolecules. 2001;34(10):3294-301.
59. Huang G, Zhang H, Liu Y, Chang H, Zhang H, Song H, et al. Strain Hardening Behavior of Poly(vinyl alcohol)/Borate Hydrogels. Macromolecules. 2017;50(5):2124-35.
60. Suzuki S, Uneyama T, Inoue T, Watanabe H. Nonlinear Rheology of Telechelic Associative Polymer Networks: Shear Thickening and Thinning Behavior of Hydrophobically Modified Ethoxylated Urethane (HEUR) in Aqueous Solution. Macromolecules. 2012;45(2):888-98.
61. Wang SQ. Transient network theory for shear-thickening fluids and physically crosslinked networks. Macromolecules. 1992;25(25):7003-10.
62. Lu T, Wang Z, Tang J, Zhang W, Wang T. A pseudo-elasticity theory to model the strain-softening behavior of tough hydrogels. Journal of the Mechanics and Physics of Solids. 2020;137:103832.
63. Eckstein F, Hudelmaier M, Putz R. The effects of exercise on human articular cartilage. J Anat. 2006;208(4):491-512.
64. Daemi H, Mashayekhi M, Pezeshki Modaress M. Facile fabrication of sulfated alginate electrospun nanofibers. Carbohydr Polym. 2018;198:481-5.
65. Ma F, Pang X, Tang B. Alginate/chondroitin sulfate based hybrid hydrogel with different molecular weight and its capacity to regulate chondrocytes activity. Carbohydrate Polymers. 2019;206:229-37.
66. Shah SA, Sohail M, Khan SA, Kousar M. Improved drug delivery and accelerated diabetic wound healing by chondroitin sulfate grafted alginate-based thermoreversible hydrogels. Materials Science and Engineering: C. 2021;126:112169.
67. Zare P, Pezeshki-Modaress M, Davachi SM, Zare P, Yazdian F, Simorgh S, et al. Alginate sulfate-based hydrogel/nanofiber composite scaffold with controlled Kartogenin delivery for tissue engineering. Carbohydrate Polymers. 2021;266:118123.
68. Goto R, Nakahata M, Sakai S. Phenol-Grafted Alginate Sulfate Hydrogel as an Injectable FGF-2 Carrier. Gels [Internet]. 2022; 8(12).
69. Tzioumis NA, Cullen DA, Jolliffe KA, White NG. Selective Removal of Sulfate from Water by Precipitation with a Rigid Bis-amidinium Compound. Angewandte Chemie International Edition. 2023;62(12):e202218360.
70. Bibi A, Rehman S-u, Yaseen A. Alginate-nanoparticles composites: kinds, reactions and applications. Materials Research Express. 2019;6(9):092001.
71. Mohamadinia P, Anarjan N. Preparation And Characterization of Sodium Alginate/Acrylic Acid Composite Hydrogels Conjugated To Silver Nanoparticles As An Antibiotic Delivery System2021.
72. Le D, Sugawara-Narutaki A. Elastin-Like Polypeptides as Building Motifs toward Designing Functional Nanobiomaterials. Molecular Systems Design & Engineering. 2019;4.
73. Nettles DL, Chilkoti A, Setton LA. Applications of elastin-like polypeptides in tissue engineering. Adv Drug Deliv Rev. 2010;62(15):1479-85.
74. Fisher SA, Baker AEG, Shoichet MS. Designing Peptide and Protein Modified Hydrogels: Selecting the Optimal Conjugation Strategy. Journal of the American Chemical Society. 2017;139(22):7416-27.
75. Varanko AK, Su JC, Chilkoti A. Elastin-Like Polypeptides for Biomedical Applications. Annual Review of Biomedical Engineering. 2020;22(1):343-69.

Acknowledgments – The author is grateful to Driesen S. for their supervision, feedback, and assistance in conducting the experiments and data analysis. The author is grateful to Penxten H., Thijssen E., Van Vinckenroye K., and Helsen A. for their technical support. The author is grateful to Arickx U. for feedback, help with statistical analysis, general support, and interchange of ideas. The author is grateful to the members of the AFP & BDG research groups for their general support and feedback. The author thanks Pitet L. and Graulus G-J. for arranging the internship, providing this opportunity, and for feedback.

Authorship contribution – Pitet L., Graulus G-J. & Driesen S. conceived and designed the research. Atella V. and Driesen S. performed experiments. Van Vinckenroyen K., Thijssen E., Helsen A., Driesen S., and Atella V. performed data collection. Data analysis was done by Driesen S. and Atella V. Writing of the paper was done by Atella V. All authors carefully edited and approved the manuscript.

■ SUPPLEMENTARY INFORMATION

Table S1 Hydrogel formulations. All hydrogels are made with a solid content of 25 wt% which consists of alginate, acrylamide, and acrylic acid. Each formulation differs in the wt% of alginate. Each formulation has an A & B variant which differ in the acrylamide:acrylic acid ratio, 80:20 and 90:10, respectively.

Gel formulation	Water (wt%)	Solid (wt%)		
		Alginate (wt%)	Acrylamide (wt%)	Acrylic acid (wt%)
1A	75	1	19.20	4.80
1B	75	1	21.60	2.40
2A	75	2	18.40	4.60
2B	75	2	20.70	2.30
3A	75	3	17.60	4.40
3B	75	3	19.80	2.20

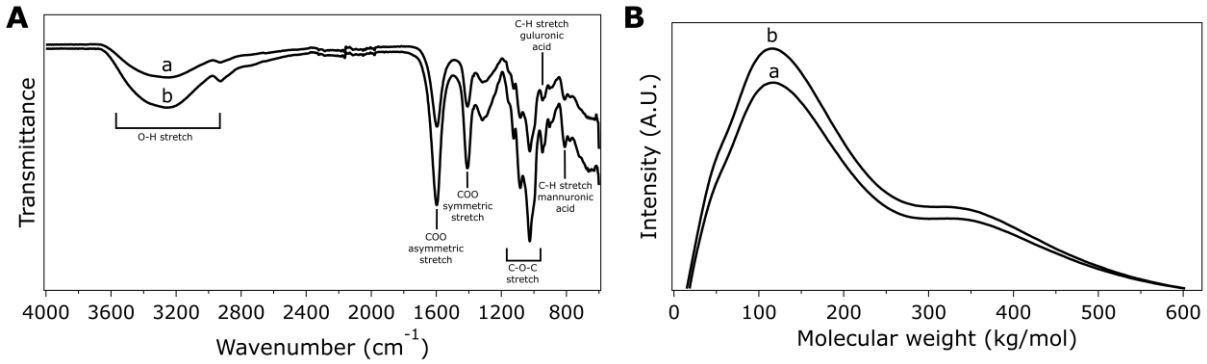

Figure S1 Characterization of purified alginate. (A) FT-IR spectra of commercial alginate and purified alginate. Both spectra are identical, showing no changes in the chemical structure of the alginate due to the purification procedure. Characteristic bands indicated at 3570-3100 cm^{-1} (O-H), 1635 cm -1 and 1419 cm^{-1} (COO), 1050-1250 cm^{-1} (C-O-C), 820 cm^{-1} and 946 cm^{-1} (C-H). **(B)** GPC chromatogram of commercial alginate and purified alginate. The molecular weight distribution is identical, once again indicating no changes to the chemical structure. The molecular weights are 130 kg/mol and 127 kg/mol for alginate and purified alginate, respectively. The dispersity's (Đ) are 1.59 and 1.65 for alginate and purified alginate, respectively.
a: commercial alginate, b: purified alginate

Table S2 Tensile properties of the six DN hydrogel formulations synthesized via the two-step method. Most A & B variants display similar properties. The max strain increases when the wt% of alginate increases from 1 to 2, but decreases at 3 wt%. The max stress also follows this trend. The elastic modulus increases with increasing alginate wt%.

Gel formulation	Max strain (%)	Max stress (kPa)	Elastic modulus (kPa)
1A	600±204	188±64	54.7±8.8
1B	644±250	230±179	36.6±21
2A	700±100	170±27	50.7±0.30
2B	863±200	348±75	99.6±1.3
3A	547±104	246±55	113±16
3B	440±308	210±96	140±36

Table S3 Tensile properties of the six DN hydrogel formulations synthesized via the one-step method. Most A & B variants display similar properties. The max strain increases when the wt% of alginate increases from 1 to 2, but decreases at 3 wt%. The max stress also follows this trend. The elastic modulus increases with increasing alginate wt%.

Gel formulation	Max strain (%)	Max stress (kPa)	Elastic modulus (kPa)
1A	903±274	330±130	59.9±8.5
1B	588±237	254±209	68.7±27
2A	1134±299	460±201	96.6±14
2B	1164±31	689±88	99.9±28
3A	665±121	248±26.5	90.8±8.1
3B	979±357	417±175	132±37

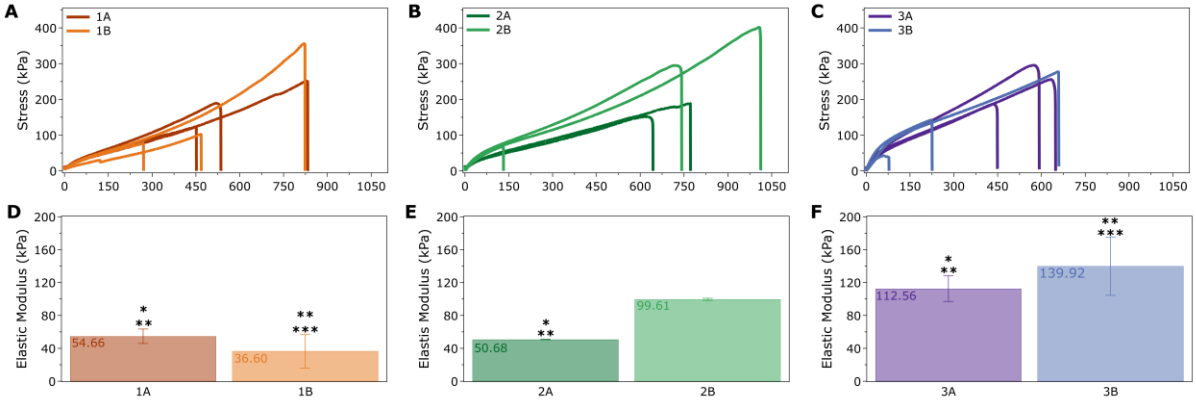

Figure S2 Tensile properties of the six DN hydrogels synthesized via the two-step method. All hydrogels display nonlinear viscoelastic behavior. **(A-C)** Tensile stress-strain curves of the A and B variants of formulations 1, 2 and 3, respectively. A general increase in the slope of the elastic region is visible as the amount of alginate increases, indicating higher degrees of toughness. Ductility is similar for formulations 1 and 2, while formulation 3 is noticeably less ductile and more rigid. **(D-F)** Elastic modulus of the A and B variants of formulations 1, 2, and 3, respectively. The moduli of the A & B variants are similar, indicating that a change in acrylic acid content does not greatly alter the toughness. A general increase in the modulus is visible as the amount of alginate increases, indicating higher degrees of toughness. However, only the indicated moduli are significantly different.
** = P ≤ 0.05, ** = P ≤ 0.01, *** = P ≤ 0.001*

Table S4 Compressive properties of the six DN hydrogels synthesized via the two-step method. All hydrogels reached 90% strain. Most A & B variants display similar properties. The max stress seems to increase when the alginate reaches 3 wt%. 1 or 2 wt% seems to have little impact on the max stress. The compressive modulus increases with alginate wt%. However, 2 or 3 wt% alginate does not seem to drastically influence the modulus. The max stress reached, and the modulus does not logically match, indicating that the random nature of plastic deformation is at the basis for the reached max stress.

Gel formulation	Max stress (MPa)	Compressive modulus (kPa)
1A	2.16±0.79	118±43
1B	2.18±0.97	123±5
2A	2.15±0.55	150±72
2B	3.24±0.68	186±93
3A	4.36±0.97	149±27
3B	2.37±0.32	163±19

Table S5 Compressive properties of the six DN hydrogels synthesized via the one-step method. All hydrogels reached 90% strain. Most A & B variants display similar properties. The max stress for the formulations with 1 wt% alginate is extraordinarily high when compared to the other formulations. The max stress increases when the alginate increases from 2 wt to 3 wt%. The compressive modulus increases with alginate wt%. The max stress reached, and the modulus does not logically match, indicating that the random nature of plastic deformation is at the basis for the reached max stress.

Gel formulation	Max stress (MPa)	Compressive modulus (kPa)
1A	7.90±2.4	223±23
1B	16.3±5.5	234±45
2A	4.77±2.4	245±58
2B	8.55±3.44	277±87
3A	9.93±2.2	376±48
3B	9.49±3.2	304±25

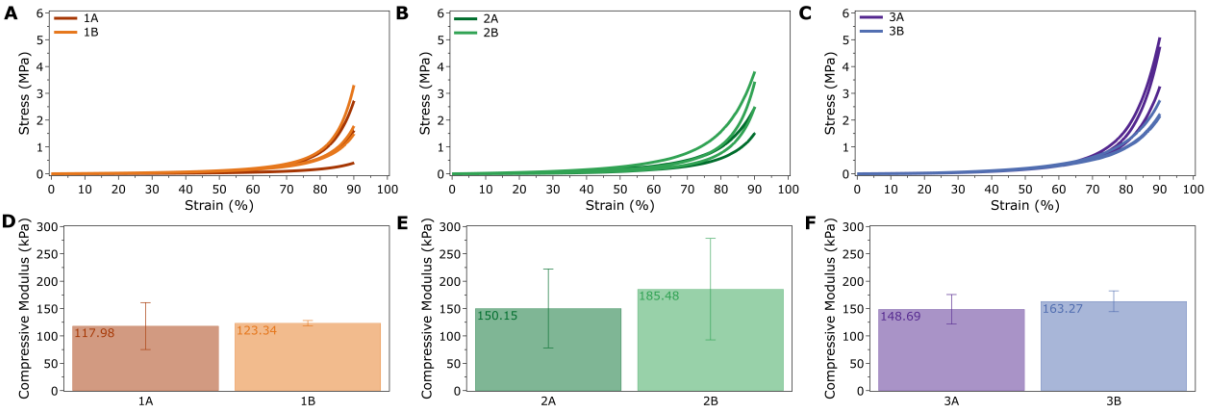

Figure S3 Compression properties of the six DN hydrogels synthesized via the two-step method. All hydrogels display nonlinear viscoelastic behavior. **(A-C)** Compression stress-strain curves of the A and B variants of formulations 1, 2, and 3, respectively. A general increase in the slope and maximum stress is visible as the amount of alginate increases, indicating higher degrees of toughness. **(D-F)** Compressive modulus of the A and B variants of formulations 1, 2, and 3, respectively. The moduli of the A & B variants are similar, indicating that a change in acrylic acid content does not greatly alter the toughness. A general increase in the modulus is visible as the amount of alginate increases, indicating higher degrees of toughness.